Deep-mantle krypton reveals Earth's early accretion of carbonaceous matter

Sandrine Péron, Sujoy Mukhopadhyay, Mark D. Kurz, David W. Graham

Title: Deep mantle krypton reveals Earth's early accretion of carbonaceous matter

Authors: Sandrine Péron[1*], Sujoy Mukhopadhyay[1], Mark D. Kurz[2], David W. Graham[3]

Author affiliations:

[1]Department of Earth and Planetary Sciences, University of California - Davis, Davis, CA 95616, United States of America

[2]Marine Chemistry and Geochemistry, MS #25, Clark 421, Woods Hole Oceanographic Institution, Woods Hole, MA 02543, United States of America

[3]College of Earth, Ocean, and Atmospheric Sciences, Oregon State University, Corvallis, OR 97331, United States of America

*scperon@ucdavis.edu

Summary paragraph:

Establishing when, and from where, carbon, nitrogen and water were delivered to Earth is a fundamental objective in understanding the origin of habitable planets like Earth. Yet volatile delivery to Earth remains controversial[1–5]. Krypton isotopes provide unique insights on volatile delivery due to significant isotopic variations among sources[6–10], although pervasive atmospheric contamination has hampered analytical efforts. Here, we use a new methodology to present the full suite of krypton isotopes from the deep mantle Galápagos and Iceland plumes with the most primitive helium, neon and tungsten isotopic compositions[11–16]. Except for ^{86}Kr, the Kr isotopic compositions are similar to a mixture of chondritic and atmospheric Kr. These results suggest early accretion of carbonaceous material by proto-Earth and rule out any combination of hydrodynamic loss with

outgassing of the deep or shallow mantle to explain atmospheric noble gases. Unexpectedly, the deep mantle sources have a deficit in the neutron-rich ^{86}Kr relative to the average composition of carbonaceous meteorites, suggesting a nucleosynthetic anomaly. Although the relative depletion of neutron-rich isotopes on Earth compared to carbonaceous meteorites has been documented for a range of refractory elements[1,17,18], our observations suggest such a depletion for a volatile element. This finding suggests that accretion of volatile and refractory elements occurred simultaneously, with krypton recording concomitant accretion of non-solar volatiles from more than one type of material, possibly including outer Solar System planetesimals.

Main Text

Volatile delivery was a key process that shaped Earth's early surface environment. Yet the timing and sources of volatile delivery, as well as subsequent volatile evolution are still debated[1–5,19]. Whereas some studies advocate for most volatile delivery before the last giant impact[5,19], a contribution from a late veneer event may also be required[1,2]. Three main sources seem to be needed to explain the Earth's volatile composition, namely solar[3,4,20], chondritic[20] and cometary[21]. The study of accretional heterogeneities preserved in the deep mantle provides direct observational constraints for testing planet formation models, in particular regarding the processes responsible for material migration in the solar system[1,3]. For instance, dual accretion of volatile-rich outer solar system material and solar gases in the deep Earth[10,22] may indicate early transport of outer solar system solids into the Earth's formation region[23].

Being inert, noble gases are ideal tracers of volatile sources and evolution[3,4]. However, the Earth's deep mantle noble gas composition remains poorly constrained, particularly for Kr and

Xe. Krypton, with its six stable isotopes, ^{78}Kr, ^{80}Kr, ^{82}Kr, ^{83}Kr, ^{84}Kr and ^{86}Kr, is extremely well-suited to deconvolve solar from chondritic sources because they have distinct isotopic compositions; solar and chondritic material being enriched in light and heavy Kr isotopes relative to Earth's atmosphere, respectively[24,25]. Upper mantle Kr appears chondritic rather than solar based on measured ^{82}Kr/^{84}Kr and ^{86}Kr/^{84}Kr ratios in CO_2 well gases[9]. Measurement of the ^{86}Kr/^{84}Kr ratio from a single mid-ocean ridge basalt (MORB) is also consistent with chondritic Kr in the upper mantle[8]. A recent investigation of deep mantle Kr and Xe isotopes in volcanic gases from the Yellowstone hotspot suggests a chondritic origin[10]. As neon isotopes in basalts derived from the deep mantle indicate acquisition of a solar component during the early phase of Earth's accretion[4,26,27], the Yellowstone results could indicate a dual solar and chondritic source during early terrestrial accretion[10]. The fingerprint of crustal and lithospheric mantle helium and neon in the Yellowstone gas samples[10], however, leaves room for the possibility that Kr in these samples may be derived from a source less primitive than other hotspots such as Hawaii, Iceland and Galápagos. In addition, the mantle compositions of the light isotopes ^{78}Kr and ^{80}Kr are not known due to their very-low abundances, ubiquitous atmospheric contamination and progressive atmospheric noble gas recycling into the mantle. As we show, these isotopes are critical for determining the volatile sources for Kr, and by inference Xe.

Deep mantle krypton and xenon

We analyzed the krypton isotopic composition of ocean island basalt (OIB) glass samples from Fernandina, Galápagos and from Midfell, Iceland. These two hotspots sample the deep mantle via plumes rooted at the core-mantle boundary[28] and the samples analyzed have the most

primitive neon compositions[11,13–16]. Furthermore, both plumes have negative tungsten isotope anomalies with Galápagos carrying the largest negative anomaly[12]. To overcome challenges of low noble gas abundances and ubiquitous shallow-level atmospheric contamination in basalts[29], we used the novel technique of accumulating Ar, Kr and Xe from crushing steps that show little atmospheric contamination as determined by analyses of neon isotopes[8], followed by an effective Ar-Kr-Xe separation and multicollection of five Kr isotopes during the mass spectrometric analyses (Methods).

The krypton isotopic compositions of Galápagos and Iceland (Extended Data Table 1) are distinct from air and solar wind but similar to the chondritic end-member (Figure 1, Extended Data Figures 1, 2). The measured $^{82}Kr/^{84}Kr$ and $^{86}Kr/^{84}Kr$ ratios of both plumes are similar to the highest measured values of the upper mantle based on CO_2 well gases[9] and one MORB[8] (Figure 2). Whether this similarity extends to the lighter isotope ratios $^{78}Kr/^{84}Kr$ and $^{80}Kr/^{84}Kr$ remains to be determined because these ratios have not been established for the upper mantle. The Galápagos and Iceland krypton ratios are similar to one sample from the Yellowstone hotspot[10] but differ from a second sample (Figure 2), the reasons for which are not entirely clear.

The xenon isotopic data of Galápagos and Iceland are reported in Extended Data Table 2 and shown in Figure 3. While there are no literature data for Galápagos, the new Iceland data are in very good agreement with literature data for xenon[14,15]. The Iceland accumulated gas is similar in composition to the error-weighted step-crush average of the DICE sample (Supplemental Figure 5)[14], which provides confidence for the krypton isotope data. However, the error-weighted DICE average[14] is closer to air because of a greater atmospheric contamination (Figure 3). The Galápagos accumulated gas is also very similar in composition to the DICE error-weighted step-crush average[14]. Importantly, our xenon data do not plot on a mass fractionation line (Figure 3).

The non-radiogenic $^{124}Xe/^{130}Xe$ and $^{126}Xe/^{130}Xe$ ratios are not resolved from air. But the Galápagos and Iceland non-radiogenic $^{128}Xe/^{130}Xe$ ratios show slight excesses relative to air. In the $^{128}Xe/^{130}Xe$ – $^{129}Xe/^{130}Xe$ space, the Galápagos average barely overlaps with the best fit mixing line between the atmosphere and upper mantle samples[8,30–32], whereas the Iceland average appears to fall on the line. While the Yellowstone plume data appear to fall on a steeper mixing line than the upper mantle[10], the uncertainty in the Galápagos and Iceland data do not allow us to conclude whether they are on the same mixing line defined by samples from the upper mantle[8,30–32] or a slightly steeper mixing line.

Recycled proportion of atmospheric Kr

The clear observation of non-atmospheric Kr in the Galápagos and Iceland sources provides firm constraints on the amount of atmospheric krypton recycled into the deep mantle through subduction[31,33]. For primordial mantle Kr, we use two meteoritic reference points, Average Carbonaceous Chondrites (AVCC; Methods and Extended Data Table 3) and Phase Q, which is a poorly characterized carbonaceous phase carrying the majority of trapped heavy noble gases in meteorites[25]. Phase Q is widespread in chondrites and usually the only trapped component in achondrites[25,34,35], while carbonaceous chondrites are the meteorite group for which there is currently the most precise Kr isotopic data. If the primordial plume source Kr composition is assumed to be equivalent to AVCC, or to Phase Q, the proportion of atmospheric Kr in the plume source would range from 64 ± 8 % to 0^{+9}_{0} % (Figure 4; Methods). Likewise, we can place upper bounds on the amount of solar Kr in the deep mantle by assuming a solar-AVCC

mixture, which constrains the solar component to be 10 ± 2 % and 16 ± 2 % of the Kr in the Galápagos and Iceland plumes, respectively (Figure 4).

The measured krypton and xenon isotopic anomalies from Galápagos and Iceland are lower limits of the isotopic anomalies in the mantle sources of these two plumes because the measured values have not been entirely corrected for shallow-level atmospheric contamination; the gas accumulation methodology drastically reduces atmospheric contamination but does not eliminate it[8] (Methods). Thus, the *maximum* proportions of recycled atmospheric krypton are 48 ± 8 % and 64 ± 8 % for the Galápagos and Iceland sources, respectively, assuming AVCC as the initial composition (Figure 4). The proportions of recycled air in the mantle plumes suggest that the Galápagos source may have retained a more primitive heavy noble gas signature than the Iceland source, consistent with the less radiogenic $^{3}He/^{4}He$ ratios, the less nucleogenic $^{21}Ne/^{22}Ne$ ratios and the more negative $\mu^{182}W$ in the Galápagos source[11–16]. Using the ^{128}Xe excesses, we estimate the maximum proportion of recycled atmospheric xenon in the deep mantle. Assuming an initial composition similar to AVCC, at maximum, 93 ± 5 % and 95^{+5}_{-6} % of the ^{130}Xe budget are of recycled origin for the Galápagos and Iceland mantle sources, respectively. The percentage of recycled ^{130}Xe in the Iceland plume based only on the $^{128}Xe/^{130}Xe$ ratio from this study is in good agreement with the $93.4^{+2.4}_{-1.2}$ % estimated previously for the Iceland plume using $^{130,131,132,134,136}Xe$[33]. As a comparison, for plume-influenced samples from the Rochambeau rift in the Lau Basin, $88.8^{+3.1}_{-1.2}$ % of ^{130}Xe is from recycling[33,36]. Importantly, the maximum proportion of recycled Kr in the plumes is lower than the minimum proportion of recycled xenon, demonstrating that krypton in the mantle is significantly less affected by recycling than xenon.

Sources of Earth's volatiles

To determine the origin of primordial Kr, we investigate the full suite of Kr isotopes, which indicates that the measured $^{78,80,82,83}Kr/^{84}Kr$ ratios in both plumes are similar to that of Phase Q[25] (Figure 1). The krypton isotopic anomalies, relative to air, are slightly lower for the Iceland sample, but within uncertainties of the Galápagos values (Figures 1 and 2).

In spite of the similarity of the light Kr isotopes with Phase Q, the initial deep mantle krypton isotopic composition cannot be derived solely from Q. The measured $\delta^{86}Kr$ for both plumes are significantly lower than the value for Q. Based on calculated proportions of a Phase Q-air mixture (Figure 4), the expected $\delta^{86}Kr$ are 14.1 ± 1.3 ‰ for Galápagos and 10.1 ± 2.6 ‰ for Iceland, significantly higher than their respective measured values of 3.09 ± 0.92 ‰ and 2.06 ± 1.17 ‰ (Figure 5).

Carbonaceous chondrites may represent a possible source of krypton, and therefore other volatiles, for the deep mantle (Figures 1 and 2). Based on the mixing proportions of AVCC-air Kr (Figure 4), the expected $\delta^{86}Kr$ is 6.85 ± 0.98 ‰ for Galápagos and 4.71 ± 0.98 ‰ for Iceland, significantly higher than the measured values (Figure 5). Given the uncertainties in the measured and predicted values, the probability that the measured $\delta^{86}Kr$ values for *both* the Galápagos and Iceland are lower than the predicted values by random chance is 0.01% (Extended Data Figure 3); that is, there is a 99.99% probability that Earth's mantle has a deficit in the heaviest Kr isotopes with respect to the average composition of carbonaceous chondrites. Given the small data set and the limited precision on Kr isotopic ratios for different carbonaceous chondrite groups (Extended Data Table 3), we cannot rule out that a specific group of carbonaceous chondrites may match the Earth's deep mantle Kr isotopic composition. However, dynamically,

several types of carbonaceous chondrite would be expected to be scattered to the inner solar system during Earth's formation.

The misfit to the deep mantle's $\delta^{86}Kr$ would be larger for ordinary and enstatite chondrites (Extended Data Table 3) because they have higher $^{86}Kr/^{84}Kr$ values than AVCC. Likewise, a mix of solar-AVCC Kr predicts significantly higher $\delta^{86}Kr$ (Figure 5). Consequently, the deep mantle has a nucleosynthetic ^{86}Kr anomaly with respect to AVCC, enstatite and ordinary chondrites, and solar compositions; the average composition of carbonaceous chondrites though provides the closest match. The nucleosynthetic ^{86}Kr anomaly is more visible in the Galápagos plume given its higher proportion of primordial krypton compared to Iceland (Figure 4).

The nucleosynthetic ^{86}Kr anomaly of the two hotspots must be a remnant of Earth's accretion, signifying that some planetary building blocks carried a lower $^{86}Kr/^{84}Kr$ ratio than represented by the AVCC composition or Phase Q. The $\delta^{86}Kr$ of s-process nucleosynthesis, determined through analyses of interstellar SiC from the Murchison carbonaceous chondrite, exhibits a wide range[37] from -223 to +3041 ‰[38], requiring several stellar sources to have contributed SiC grains to the parent molecular cloud of the Solar System[38]. The large variability in $\delta^{86}Kr$ of SiC grains occurs as ^{86}Kr is at a branching point on the s-process path. Incomplete mixing of SiC grains, derived from AGB stars, in the solar nebula might then have imparted varying $^{86}Kr/^{84}Kr$ ratios in different parent bodies with some carrying ^{86}Kr depletion relative to the average composition of carbonaceous chondrites. However, we cannot rule out the possibility that r-process nucleosynthesis associated with supernovae may also have produced variability in the neutron-rich Kr isotopic ratio as ^{86}Kr is not shielded from r-process nucleosynthesis.

Several refractory elements (e.g., Ca, Ti, Cr, Ni, Zr, Mo, Ru, and Nd) on Earth exhibit relative depletions in neutron-rich isotopes in reference to carbonaceous meteorites[1,17,18]. These

depletions have been attributed to a relative enrichment of s-process over r-process matter, as well as to heterogeneous distribution of grains derived from different AGB stars in Earth-forming materials[1,17,18]. Isotopes of refractory elements like Ca and Ti track the composition of accreted material throughout Earth's formation[17,39]. Hence, the observed relative depletion in a neutron-rich isotope for the highly volatile element Kr in the solid Earth (Figure 5) suggests that its depletion may be linked to relative depletion of the neutron-rich refractory elements on Earth, indicating accretion of volatile and refractory elements occurred simultaneously.

Earth's deep mantle deficit in ^{86}Kr has ramifications for the longstanding debate about the origin of terrestrial xenon as the heavy noble gases (Kr, Xe) are thought to have a common origin on Earth[9,10]. The initial xenon in Earth's mantle and atmosphere was long advocated to be U-Xe[40], a primordial component with a deficit in the neutron-rich isotopes ^{134}Xe and ^{136}Xe[41], but never directly observed in a parent body. Recently, U-Xe was shown to be a mixture of chondritic and cometary Xe[21], establishing an observational basis for the Earth's initial atmospheric composition. On the other hand, for the mantle, chondritic Xe, and not U-Xe, has been suggested as the progenitor[8–10], although differences between chondritic and U-Xe are not discernible given the measurement uncertainties. Instead, the Kr isotopic results suggest that the Earth's mantle may well have a deficit of the neutron-rich Xe isotopes with respect to chondrites; i.e., a U-Xe pattern reflecting a mixture of chondritic and cometary Xe[21].

To further evaluate the possible sources of deep mantle Kr, we investigate the nature of the accretionary material. Earth may have primarily grown from differentiated planetesimals as sampled in achondrites[42]. In differentiated meteorites, Kr is mainly hosted in Phase Q[25,34]. Although it is unlikely that deep mantle Kr is only from Phase Q (Figures 4, 5). If Earth grew from differentiated planetesimals, then either the achondrite parent bodies had significantly lower

$^{86}Kr/^{84}Kr$ ratios than Phase Q due to the presence of other nucleosynthetic components, unlike those that have been observed[25,34,35], or additional parent bodies with a low $^{86}Kr/^{84}Kr$ ratio were also added. The nature of the ^{86}Kr-depleted parent body is not entirely clear. The only planetary body that has so far been shown to carry a deficit in ^{86}Kr relative to solar wind is the Kuiper Belt comet 67P/C-G[43]. Accretion of cometary material would also have produced a depletion in the heavy Xe isotopes[21], leading to a U-Xe composition of the deep mantle. Due to the large uncertainty in the cometary krypton composition[43] a mixing calculation to determine the proportion of cometary Kr required to explain the deep mantle Kr isotopic composition is not feasible.

The measured Kr isotopic composition may be explained by accretion of a specific group of carbonaceous chondrites, or parent bodies carrying noble gases in the carbonaceous phase Q, such as enstatite or ordinary chondrites[25], with other parent bodies, potentially comets, carrying a depletion in the neutron-rich ^{86}Kr isotope. The enstatite or ordinary chondrite parent bodies would require a larger contribution from a parent body depleted in ^{86}Kr. However, since Phase Q is carbonaceous and widespread in chondrites and achondrites[25,34], all scenarios require early accretion of carbonaceous phases. The discussions above highlight that one or more volatile-rich outer solar system objects likely contributed to the deep mantle's krypton budget during the earliest phase of Earth's accretion.

Implications for origin of atmosphere

The primordial krypton sampled by the mantle plumes had to be delivered during the early phases of Earth accretion. Indeed, mantle plumes sample a reservoir that differentiated from

the upper mantle prior to the end of Earth's main phase of accretion (i.e., by 4.45 Ga ago) and has never been homogenized with the rest of the mantle based on its ε^{182}W, I/Pu-derived Xe, and ^{3}He/^{22}Ne ratios[14,33,36]. Early Kr delivery associated with carbonaceous phases, or chondritic parent bodies, also suggests simultaneous delivery of other chondritic volatiles. This early delivery was concurrent with acquisition of solar neon in the deep mantle[10,22]. As the solar wind and solar nebula are enriched by several orders of magnitude in neon relative to krypton and because the solar Ne/Kr ratio is also several orders of magnitude higher than in chondrites, acquisition of solar neon would not affect the Kr composition[10,44,45]. We propose that the composition of volatile elements suggest delivery was not restricted towards the end of the accretion, or to the aftermath of the Moon-forming giant impact. Rather, volatile delivery may have occurred through most of Earth's accretion with volatile abundances on the growing planet sculpted and fractionated by processes such as core formation and atmospheric loss.

Volatile delivery during only the early or main phase of Earth's accretion, however, does not explain the atmospheric noble gases, the largest reservoir of noble gases on Earth. Degassing of chondritic krypton from the upper mantle does not match the atmospheric composition (Figure 2). Since hydrodynamic escape would leave a residual atmosphere enriched in the heavier isotopes, degassing of the upper mantle followed by hydrodynamic escape also cannot explain the atmospheric composition[9]. Similarly, the deep mantle enrichment in heavy Kr isotopes compared to the atmosphere (Figures 1, 2) indicates that any combination of deep and shallow mantle outgassing followed by hydrodynamic escape will not produce the atmospheric composition. The chemical similarity between the Earth and the Moon is used to argue for isotopic equilibration between the Earth's mantle and the impacting body, either through a silicate vapor disk[46] or through a synestia like planetary structure generated by vaporizing a

portion of the silicate Earth through high angular momentum impacts[47]. If isotopic equilibration of refractory lithophile isotopes between the Earth's silicate mantle and the impactor was achieved, the pre-existing atmosphere on the Earth should also have equilibrated with its silicate interior. Hence, we hypothesize that a large fraction of atmospheric noble gases was delivered after the last major equilibration of the mantle with the atmosphere, the Moon-forming giant impact[46,47]. Consequently, volatile delivery during the late veneer is also required to explain the atmospheric noble gases[9,48].

The recognition of the deep mantle's krypton isotopic patterns suggests an outer Solar System contribution to Earth's volatile budget starting early in Earth's accretion history. Carbonaceous or organic-rich material could have been delivered to the inner solar system during radial transport of dust-sized grains in the disk prior to the formation of Jupiter[49]. Additionally, during giant planet formation and migration in the nebula, volatile-rich planetesimals from the outer solar system could have been scattered onto terrestrial planet-crossing orbits[23,50]. In either scenario volatile-rich material from the outer Solar System was delivered into the terrestrial planet forming region during the early periods of Earth's accretion.

References

1. Fischer-Gödde, M. *et al.* Ruthenium isotope vestige of Earth's pre-late-veneer mantle preserved in Archaean rocks. *Nature* **579**, 240–244 (2020).
2. Albarède, F. Volatile accretion history of the terrestrial planets and dynamic implications. *Nature* **461**, 1227–1233 (2009).
3. Mukhopadhyay, S. & Parai, R. Noble Gases: A Record of Earth's Evolution and Mantle Dynamics. *Annu. Rev. Earth Planet. Sci.* **47**, 389–419 (2019).
4. Moreira, M. Noble Gas Constraints on the Origin and Evolution of Earth's Volatiles. *Geochemical Perspect.* **2**, 229–403 (2013).
5. Clay, P. L. *et al.* Halogens in chondritic meteorites and terrestrial accretion. *Nature* **551**, 614–618 (2017).
6. Ozima, M. & Zashu, S. Solar-type Ne in Zaire cubic diamonds. *Geochim. Cosmochim.*

Acta **52**, 19–25 (1988).
7. Ozima, M. & Zashu, S. Noble gas state of the ancient mantle as deduced from noble gases in coated diamonds. *Earth Planet. Sci. Lett.* **105**, 13–27 (1991).
8. Péron, S. & Moreira, M. Onset of volatile recycling into the mantle determined by xenon anomalies. *Geochemical Perspect. Lett.* **9**, 21–25 (2018).
9. Holland, G., Cassidy, M. & Ballentine, C. J. Meteorite Kr in Earth's Mantle Suggests a Late Accretionary Source for the Atmosphere. *Science* **326**, 1522–1525 (2009).
10. Broadley, M. W. *et al.* Identification of chondritic krypton and xenon in Yellowstone gases and the timing of terrestrial volatile accretion. *Proc. Natl. Acad. Sci.* 202003907 (2020). doi:10.1073/pnas.2003907117
11. Péron, S. *et al.* Neon isotopic composition of the mantle constrained by single vesicle analyses. *Earth Planet. Sci. Lett.* **449**, (2016).
12. Mundl-Petermeier, A. *et al.* Anomalous 182W in high 3He/4He ocean island basalts: Fingerprints of Earth's core? *Geochim. Cosmochim. Acta* **271**, 194–211 (2020).
13. Kurz, M. D., Curtice, J., Fornari, D., Geist, D. & Moreira, M. Primitive neon from the center of the Galapagos hotspot. *Earth Planet. Sci. Lett.* **286**, 23–34 (2009).
14. Mukhopadhyay, S. Early differentiation and volatile accretion recorded in deep-mantle neon and xenon. *Nature* **486**, 101–104 (2012).
15. Trieloff, M., Kunz, J., Clague, D. A., Harrison, D. & Allègre, C. J. The Nature of pristine noble gases in mantle plumes. *Science* **288**, 1036–1038 (2000).
16. Harrison, D., Burnard, P. & Turner, G. Noble gas behaviour and composition in the mantle: constraints from the Iceland Plume. *Earth Planet. Sci. Lett.* **171**, 199–207 (1999).
17. Render, J., Fischer-Gödde, M., Burkhardt, C. & Kleine, T. The cosmic molybdenum-neodymium isotope correlation and the building material of the Earth. *Geochemical Perspect. Lett.* **3**, 170–178 (2017).
18. Akram, W., Schönbächler, M., Bisterzo, S. & Gallino, R. Zirconium isotope evidence for the heterogeneous distribution of s-process materials in the solar system. *Geochim. Cosmochim. Acta* **165**, 484–500 (2015).
19. Hirschmann, M. M. & Dasgupta, R. The H/C ratios of Earth's near-surface and deep reservoirs, and consequences for deep Earth volatile cycles. *Chem. Geol.* **262**, 4–16 (2009).
20. Marty, B. The origins and concentrations of water, carbon, nitrogen and noble gases on Earth. *Earth Planet. Sci. Lett.* **313--314**, 56–66 (2012).
21. Marty, B. *et al.* Xenon isotopes in 67P/Churyumov-Gerasimenko show that comets contributed to Earth's atmosphere. *Science* **356**, 1069–1072 (2017).
22. Harper, C. L. & Jacobsen, S. B. Noble gases and Earth's accretion. *Science* **273**, 1814–1818 (1996).
23. O'Brien, D. P., Walsh, K. J., Morbidelli, A., Raymond, S. N. & Mandell, A. M. Water delivery and giant impacts in the 'Grand Tack' scenario. *Icarus* **239**, 74–84 (2014).
24. Meshik, A., Hohenberg, C., Pravdivtseva, O. & Burnett, D. Heavy noble gases in solar wind delivered by Genesis mission. *Geochim. Cosmochim. Acta* **127**, 326–347 (2014).
25. Busemann, H., Baur, H. & Wieler, R. Primordial noble gases in 'phase Q' in carbonaceous and ordinary chondrites studied by closed-system stepped etching. *Meteorit. Planet. Sci.* **35**, 949–973 (2000).
26. Williams, C. D. & Mukhopadhyay, S. Capture of nebular gases during Earth's accretion is

preserved in deep-mantle neon. *Nature* **565**, 78–81 (2019).
27. Yokochi, R. & Marty, B. A determination of the neon isotopic composition of the deep mantle. *Earth Planet. Sci. Lett.* **225**, 77–88 (2004).
28. French, S. W. & Romanowicz, B. Broad plumes rooted at the base of the Earth's mantle beneath major hotspots. *Nature* **525**, 95 (2015).
29. Ballentine, C. J. & Barfod, D. N. The origin of air-like noble gases in MORB and OIB. *Earth Planet. Sci. Lett.* **180**, 39–48 (2000).
30. Caffee, M. W. *et al.* Primordial Noble Gases from Earth's Mantle: Identification of Primitive Volatile Component. *Science* **285**, 2115–2118 (1999).
31. Holland, G. & Ballentine, C. J. Seawater subduction controls the heavy noble gas composition of the mantle. *Nature* **441**, 186–191 (2006).
32. Bekaert, D. V, Broadley, M. W., Caracausi, A. & Marty, B. Novel insights into the degassing history of Earth's mantle from high precision noble gas analysis of magmatic gas. *Earth Planet. Sci. Lett.* **525**, 115766 (2019).
33. Parai, R. & Mukhopadhyay, S. The evolution of MORB and plume mantle volatile budgets: Constraints from fission Xe isotopes in Southwest Indian Ridge basalts. *Geochemistry, Geophys. Geosystems* **16**, 719–735 (2015).
34. Busemann, H. & Eugster, O. The trapped noble gas component in achondrites. *Meteor. Planet. Sci.* **37**, 1865–1891 (2002).
35. Broadley, M. W., Bekaert, D. V, Marty, B., Yamaguchi, A. & Barrat, J.-A. Noble gas variations in ureilites and their implications for ureilite parent body formation. *Geochim. Cosmochim. Acta* **270**, 325–337 (2020).
36. Pető, M. K., Mukhopadhyay, S. & Kelley, K. A. Heterogeneities from the first 100 million years recorded in deep mantle noble gases from the Northern Lau Back-arc Basin. *Earth Planet. Sci. Lett.* **369–370**, 13–23 (2013).
37. Ott, U., Begemann, F., Yang, J. & Epstein, S. S-process krypton of variable isotopic composition in the Murchison meteorite. *Nature* **332**, 700–702 (1988).
38. Lewis, R. S., Amari, S. & Anders, E. Interstellar grains in meteorites: II. SiC and its noble gases. *Geochim. Cosmochim. Acta* **58**, 471–494 (1993).
39. Dauphas, N. The isotopic nature of the Earth's accreting material through time. *Nature* **541**, 521 (2017).
40. Pepin, R. O. & Porcelli, D. Xenon isotope systematics, giant impacts, and mantle degassing on the early Earth. *Earth Planet. Sci. Lett.* **250**, 470–485 (2006).
41. Pepin, R. O. On the origin and early evolution of terrestrial planet atmospheres and meteoritic volatiles. *Icarus* **92**, 2–79 (1991).
42. Carlson, R. W. *et al.* How Did Early Earth Become Our Modern World? *Annu. Rev. Earth Planet. Sci.* **42**, 151–178 (2014).
43. Rubin, M. *et al.* Krypton isotopes and noble gas abundances in the coma of comet 67P/Churyumov-Gerasimenko. *Sci. Adv.* **4**, (2018).
44. Mazor, E., Heymann, D. & Anders, E. Noble gases in carbonaceous chondrites. *Geochim. Cosmochim. Acta* **34**, 781–824 (1970).
45. Heber, V. S. *et al.* Noble gas composition of the solar wind as collected by the Genesis mission. *Geochim. Cosmochim. Acta* **73**, 7414–7432 (2009).
46. Pahlevan, K. & Stevenson, D. J. Equilibration in the aftermath of the lunar-forming giant impact. *Earth Planet. Sci. Lett.* **262**, 438–449 (2007).

47. Lock, S. J. & Stewart, S. T. The structure of terrestrial bodies: Impact heating, corotation limits, and synestias. *J. Geophys. Res. Planets* **122**, 950–982 (2017).
48. Bekaert, D. V, Broadley, M. W. & Marty, B. The origin and fate of volatile elements on Earth revisited in light of noble gas data obtained from comet 67P/Churyumov-Gerasimenko. *Sci. Rep.* **10**, 5796 (2020).
49. Ciesla, F. J. & Cuzzi, J. N. The evolution of the water distribution in a viscous protoplanetary disk. *Icarus* **181**, 178–204 (2006).
50. Raymond, S. N. & Izidoro, A. Origin of water in the inner Solar System: Planetesimals scattered inward during Jupiter and Saturn's rapid gas accretion. *Icarus* **297**, 134–148 (2017).

Figure 1: **Krypton isotopic patterns of Galápagos and Iceland samples.** Isotopic ratios are in delta notation, $\delta^{i}Kr = (({}^{i}Kr/{}^{84}Kr)_{sample} / ({}^{i}Kr/{}^{84}Kr)_{air} - 1) \times 10^{3}$. The average Kr isotopic compositions of the four Galápagos and the two Iceland measurements are compared to Phase Q[25], Average Carbonaceous Chondrites (AVCC) and Solar Wind[24]. The measured Kr isotopic ratios in the Galápagos and Iceland plume sources are close to Phase Q[25]; compared to $\delta^{78}Kr$ and $\delta^{80}Kr$ of -9.9 ± 4.9 ‰ and -5.8 ± 1.8 ‰ for Phase Q[25], the Galápagos values are -10.5 ± 2.9 ‰ and -7.1 ± 2.3‰, respectively. For Iceland, $\delta^{78}Kr$ and $\delta^{80}Kr$ are -8.7 ± 3.8 ‰ and -3.0 ± 2.7 ‰, respectively. The error bars are 1σ.

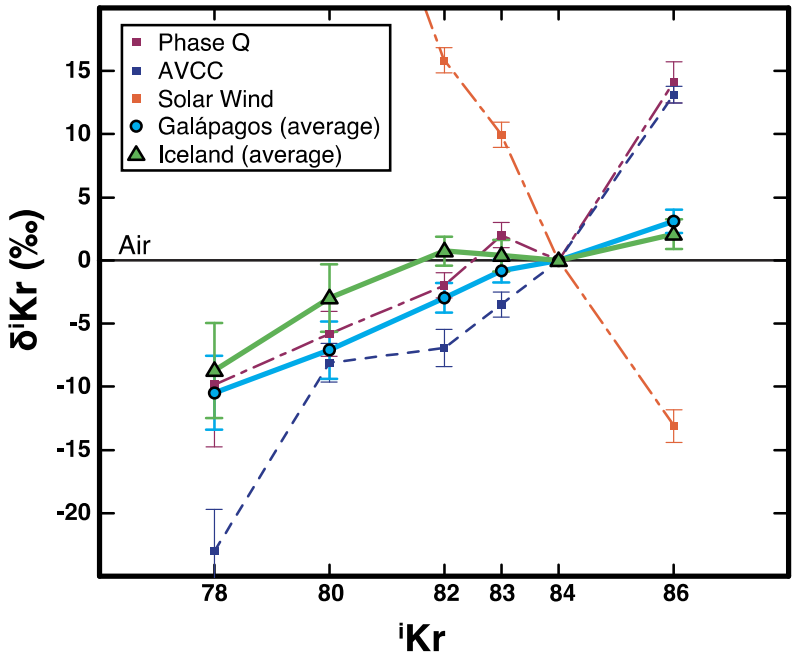

Figure 2: **Krypton isotopic compositions of Galápagos and Iceland samples.** a) $\delta^{78}Kr$ vs $\delta^{80}Kr$, b) $\delta^{82}Kr$ vs $\delta^{83}Kr$, c) $\delta^{78}Kr$ vs $\delta^{86}Kr$ and d) $\delta^{82}Kr$ vs $\delta^{86}Kr$. The Galápagos and Iceland data are the averages of the four D22 and two DG2017 measurements, respectively. Air, Phase Q[25], Average Carbonaceous Chondrites (AVCC, Extended Data Table 3) and Solar Wind[24] are shown for comparison. Data for CO_2 well gases (corrected for crustal fission) and Yellowstone are also indicated, but only ^{82}Kr, ^{83}Kr ^{84}Kr and ^{86}Kr have been measured[9,10]. The solid lines in c) and d) highlight the deficit in ^{86}Kr relative to the chondritic end-member. The measured $\delta^{82}Kr$ and $\delta^{86}Kr$ of the two mantle plumes ($\delta^{82}Kr$ of -2.9 ± 1.2 ‰ and 0.7 ± 1.1 ‰, $\delta^{86}Kr$ of 3.1 ± 0.9 ‰ and 2.1 ± 1.2 ‰ for Galápagos and Iceland, respectively) are similar to the highest measured $\delta^{82}Kr$ (-0.44 ± 0.46 ‰) and $\delta^{86}Kr$ (3.17 ± 1.44 ‰) ratios of the upper mantle based on analyses of CO_2 well gases[9] and to the $\delta^{86}Kr$ (2.29 ± 2.29 ‰, purple bar in panels c and d) of the Mid-Atlantic Ridge popping rock basalt[8]. Data for the Galápagos and Iceland hotspots rule out any solar contribution for heavy noble gases in the deep mantle. The error bars are 1□.

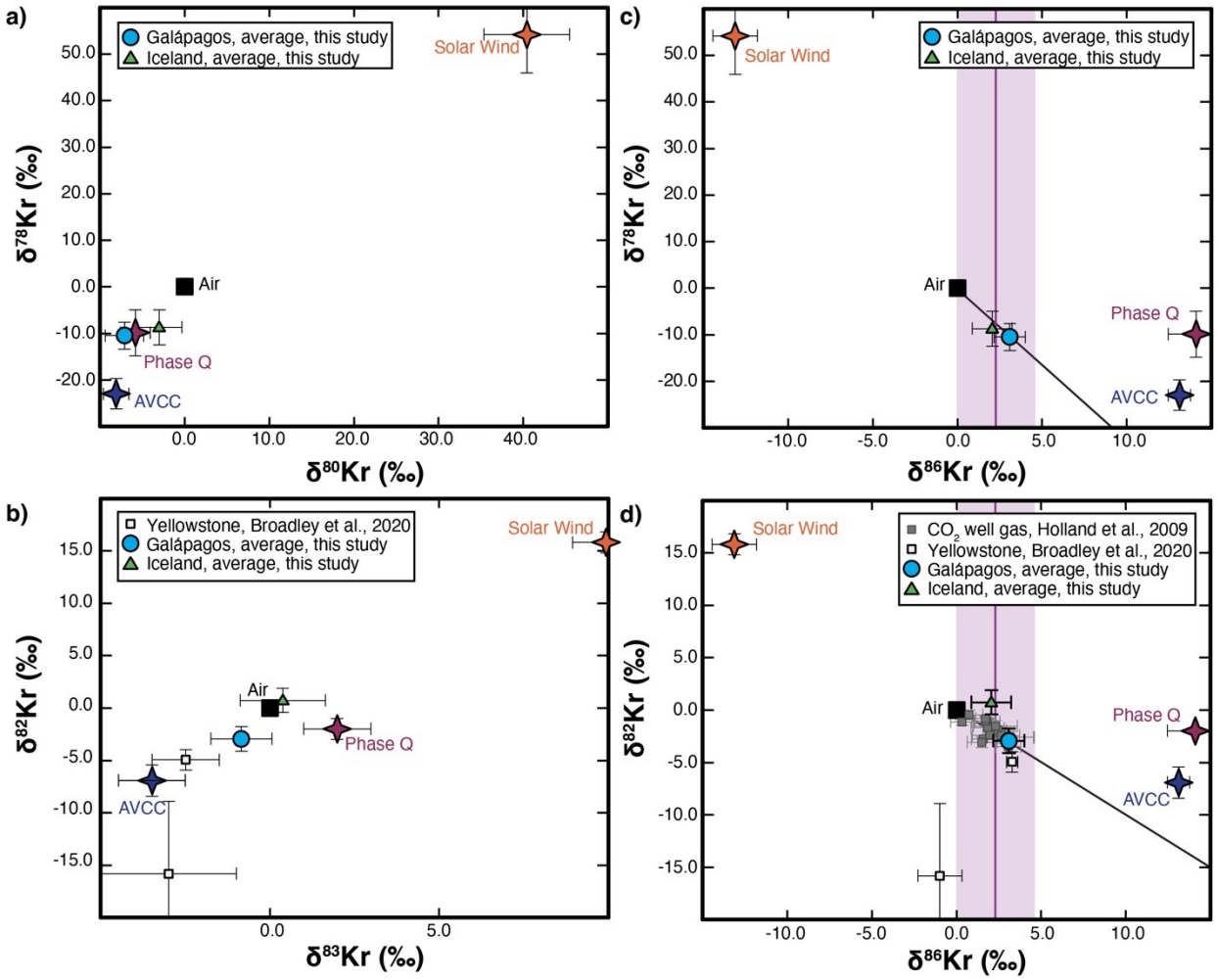

Figure 3. Xenon isotope composition of Galápagos and Iceland samples. a) $^{128}Xe/^{130}Xe$ – $^{129}Xe/^{130}Xe$, the Galápagos and Iceland data are the averages of the four D22 (small circles) and two DG2017 (small triangles) measurements, respectively. Literature data for upper mantle-derived samples from CO_2 well gases[30,31], the Mid-Atlantic Ridge popping rock basalt[8], thermal springs from Eifel[32], and for plume source samples from Iceland (error-weighted average of all crush steps of DICE)[14] and from Yellowstone[10] are shown for comparison. Data for Eifel[32] and Yellowstone[10] are normalized to the same atmospheric composition used in this study (Extended Data Table 2). *mfl* stands for mass fractionation line (dashed line). Our data for Galápagos and Iceland (averages and individual data points) are not on the *mfl*. The solid and dashed grey lines represents the mixing line (error-weighted fit forced through air) defined by upper mantle-derived samples with the 68% confidence interval. b) $^{136}Xe/^{130}Xe$ – $^{129}Xe/^{130}Xe$, the plume samples (this study, DICE error-weigthed average[14], Rochambeau error-weighted average[36] and Yellowstone[10]) in comparison with upper mantle samples (refer to Methods for references). The error bars on measurements are 1□.

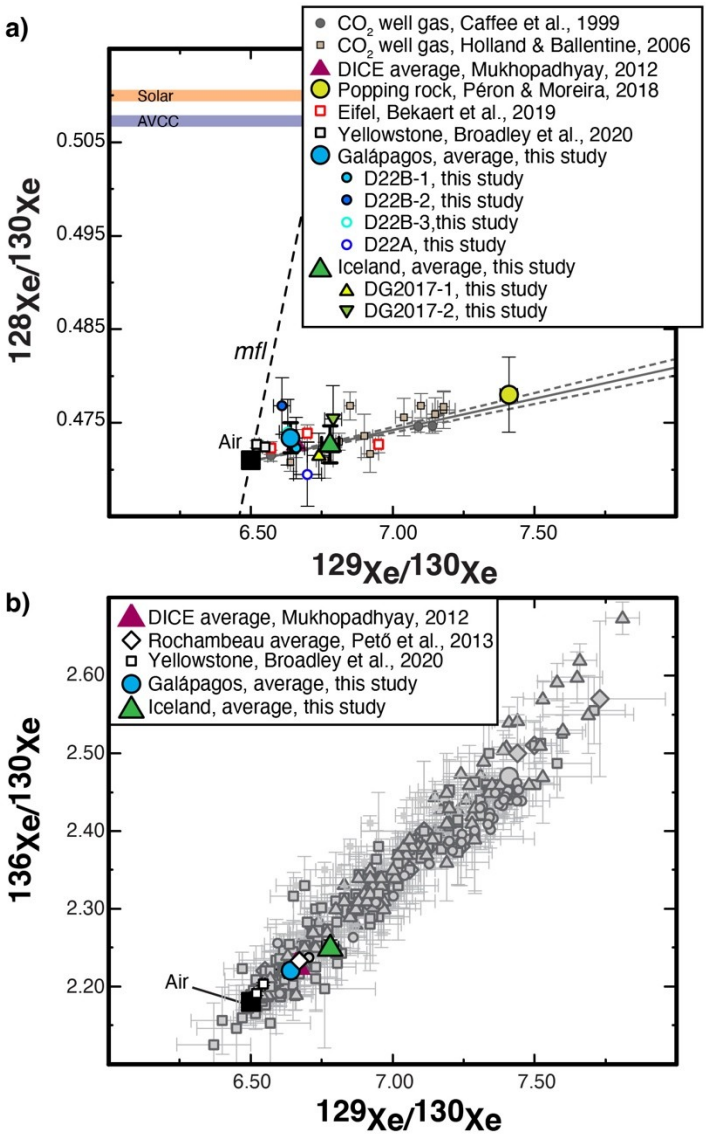

Figure 4. Mixing proportions in the plume sources. Estimates of mixing proportions to explain the ^{78}Kr-^{80}Kr-^{84}Kr compositions of samples D22A and D22B (Galápagos) and DG2017 (Iceland). Three scenarios have been considered: mixing of AVCC with air, mixing of AVCC with a solar end-member, and mixing of Phase Q with air. The error bars are 1□.

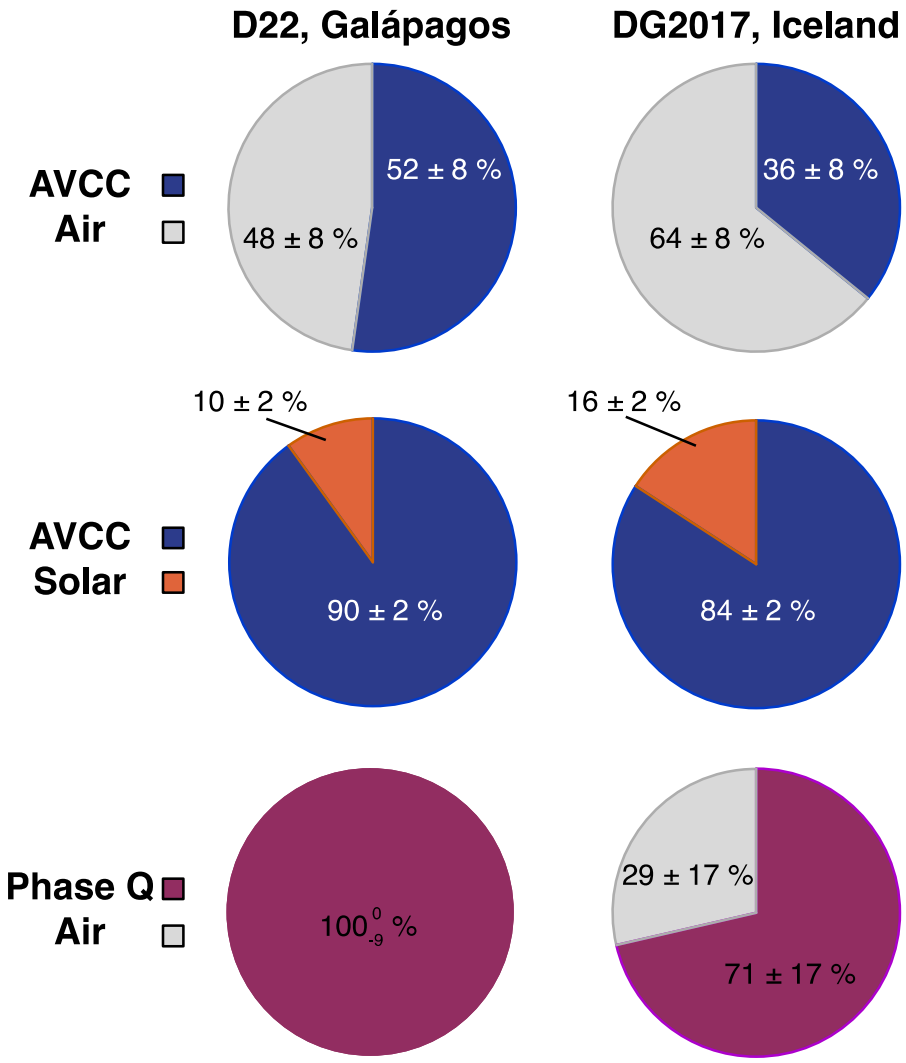

Figure 5. Estimated $^{86}Kr/^{84}Kr$ ratio based on different mixing scenarios. Predicted $^{86}Kr/^{84}Kr$ ratio (expressed in delta unit, permil deviation relative to the air ratio) based on the calculated mixing proportions (Figure 4) for samples D22 from Galápagos (left) and DG2017 from Iceland (right). These predicted ratios are compared to the average measured ratios for each sample. The comparison shows that the measured $^{86}Kr/^{84}Kr$ ratios are lower than expected based on the measured ^{78}Kr and ^{80}Kr anomalies. The error bars are 1□.

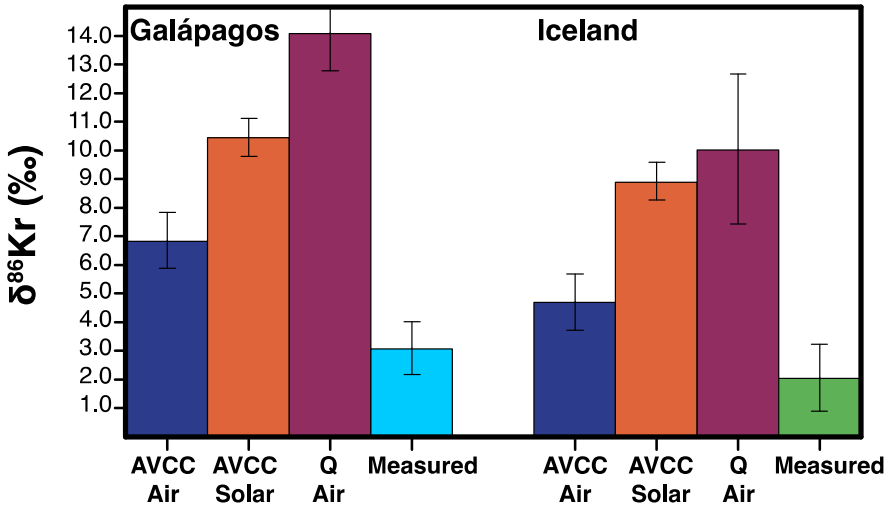

Methods

Samples

We used centimeter-sized basaltic glass chunks of samples AHA-NEMO2-D22A and AHA-NEMO2-D22B from a submarine lava flow of Fernandina volcano, Galápagos[13,51]. The composition of these samples for major, trace and volatile (major and noble gases) elements have been well characterized[11,13,51,52]. In particular, these samples have the most primitive helium and neon isotopic ratios of the Galápagos hotspot[11,13].

The Iceland sample DG2017 is a picritic sub-glacial basalt glass from Dagmalafell (Midfell), located approximately 1 km east of Lake Þingvallavatn. GPS coordinates are 64°10'29.3"N, 21°02'52.1"W. This sample was collected by Adam Kent in 2017 from the same locality as the DICE10 sample analyzed previously[16], from a small quarry at the base of a hill formed by subglacial eruptions. The sample material was taken from a mass of pillow basalts, more than 50 m high that underlies hyaloclastite. Abundances of CO_2 and He as well as the helium isotopic ratio for sample DG2017, measured by crushing and melting at OSU[53], are shown in Supplementary Table 1, and are consistent with previous studies[14–16,54]. The helium isotope ratio of DICE10, as measured at OSU, is the same within uncertainties as measured for the DG2017 sample. Abundances and isotopic compositions of Ne, Ar, Xe have also been reported for this locality[14–16,54].

Glass chunks from Galápagos and Iceland were cleaned in oxalic acid (1 %) on a hot plate (50 °C) and then rinsed with ethanol and acetone in ultrasonic baths. About 4 g (Extended Data

539 Table 1, Supplementary Table 2) of each sample were then put into crushers, that were then
540 baked between 110-120 °C for 24 hours and pumped for a minimum of 4 weeks before starting
541 the analyses. Analyses were started when the crusher blanks were below $1.0x10^{-13}$ ccSTP of ^{22}Ne,
542 $4.6x10^{-12}$ ccSTP of ^{36}Ar, $4.5x10^{-14}$ ccSTP of ^{84}Kr and $1.1x10^{-15}$ ccSTP of ^{130}Xe.
543
544 **Protocol of accumulation and noble gas purification**
545 We used a recently developed accumulation protocol[8], consisting in accumulating heavy
546 noble gases (Ar, Kr, Xe) only for crushing steps showing little atmospheric contamination as
547 determined by the prior analyses of neon isotopic ratios $^{20}Ne/^{22}Ne$ and $^{21}Ne/^{22}Ne$.
548 For each crushing step, gases were first purified successively with a hot (400 °C) MP10
549 SAES getter and then with a cold (room temperature) MP10 SAES getter. After purification,
550 gases were trapped on a dual cryogenic trap[55]. The latter is a new cryogenic system composed of
551 two electropolished stainless steel traps on one cold head[55]. One trap can be cooled to < 5 K
552 (hereafter trap A) and the other trap to < 50 K (hereafter trap B). The nude stainless steel traps
553 present steeper release curves for noble gases than charcoal traps[56], allowing a better Ar/Kr/Xe
554 separation[55].
555 Noble gases, except He, were then trapped on trap A at 9 K. A temperature cycle of the
556 trap was then conducted, consisting in putting the trap at 35 K for five minutes and then cooling it
557 down to 9 K. This temperature cycle is effective in limiting the effect of cryotrapping (the process
558 by which one noble gas is trapped by another one) as it can better re-layer each noble gas under
559 each other on the trap[57]. This operation allows recovery of a higher fraction of each noble gas.
560 Neon was then released at 25 K and introduced to the Noblesse mass spectrometer for analysis
561 (see below).

If the $^{20}Ne/^{22}Ne$ ratio of the crushing step was higher than 11.75 (and 11.49 for one step, Supplementary Table 2), then the heavy noble gases on trap A were released at 160 K and trapped on a charcoal trap at liquid nitrogen temperature (77 K) for accumulation.

To analyze the composition of the accumulated gas, the charcoal trap was first heated with a Kapton heater at 40 °C to release all the xenon. The accumulated gas was first purified with the two hot and cold MP10 SAES getters. Then gases were trapped on trap B at 67 K. The protocol then used to separate Ar/Kr/Xe is the protocol 2 described in another study[55] for samples D22B-1, D22B-1 and DG2017-1. For the three other analyses, two temperature cycles were applied for Ar/Kr and Kr/Xe separation (similar to protocol 3 of a previous study[55]) to further improve the efficiency of the separation.

Neon, argon and xenon data for the samples are indicated in Extended Data Tables 2 and 4 and Supplementary Table 2.

The charcoal trap, used to accumulate Ar, Kr, Xe from several crushing steps (Supplementary Table 2), remained several days in static vacuum. In total, the charcoal trap remained 6 days in static vacuum (isolated) for sample D22B-1, 5 days for D22B-2, 5 days for D22B-3, 3 days for D22A, 7 days for DG2017-1 and 3 days for DG2017-2. The blank of the charcoal trap after several days in static vacuum is discussed below.

Noble gas analyses on the Noblesse 5F5M

To measure the noble gas abundances and isotopic ratios, we use a Noblesse HR mass spectrometer (Nu Instruments) equipped with five faraday cups and five electron multipliers (5F5M) at the Davis Noble Gas Laboratory. Filament voltage was kept at – 78 V and the trap current at 250 μA for all the analyses.

585 Neon isotopes, ^{20}Ne, ^{21}Ne and ^{22}Ne, were measured in multicollection on electron
586 multipliers, on the right side of the peaks where ^{20}Ne is resolved from $^{40}Ar^{++}$. Signals of HF and at
587 mass 44 were measured to correct for HF^+ and CO_2^{++} interferences, using the measured
588 double/single charge ratios CO_2^{++}/CO_2^+ of 0.0068 ± 0.0005.

589 Argon isotopes were measured in multicollection, ^{40}Ar on one of the Faraday cups and
590 ^{36}Ar and ^{38}Ar on electron multipliers.

591 Krypton isotopes were measured in two steps on electron multipliers. The first step
592 consisted in measuring in multicollection ^{78}Kr, ^{80}Kr, ^{82}Kr, ^{84}Kr and ^{86}Kr, the second step in
593 analyzing ^{83}Kr. Measurements were done on the left side of the peaks, where interferences with
594 hydrocarbon on krypton isotopes are resolved. The isotope ^{80}Kr was measured on the electron
595 multiplier that has a slit (initially for resolving ^3He from HD) that allows full resolution of ^{80}Kr
596 from any interfering hydrocarbons. Kr is efficiently separated from Ar using the dual stainless
597 steel trap[55]. As a result, no interference of $^{40}Ar_2^+$ with ^{80}Kr was detected (see discussion below).

598 Xenon isotopes were measured in three steps on electron multipliers, the first step for
599 ^{126}Xe, ^{129}Xe, ^{132}Xe, the second step for ^{128}Xe, ^{131}Xe, ^{134}Xe and the third step for ^{124}Xe, ^{130}Xe, ^{136}Xe.
600

601 **Sensitivity, reproducibility and mass discrimination of the measurements**

602 Sensitivity, reproducibility and mass discrimination of the measurements were assessed
603 through repeat analyses of air standards of similar size as the samples. Each pipette of the air
604 standard corresponds to 6.15×10^{-11} ccSTP of ^{22}Ne, 1.15×10^{-9} ccSTP of ^{36}Ar, 2.38×10^{-11} ccSTP of
605 ^{84}Kr and 1.30×10^{-13} ccSTP of ^{130}Xe.

606 Typical values of sensitivity of the mass spectrometer during the analysis periods were
607 $1.1x10^{-14}$ cm^3/cps for ^{22}Ne, $1.9x10^{-15}$ cm^3/cps for ^{36}Ar, $4.8\text{-}5.0x10^{-16}$ cm^3/cps for ^{84}Kr and 4.6-
608 $5.1x10^{-16}$ cm^3/cps for ^{130}Xe.

609 Extended Data Figure 4 shows the measurement reproducibility of air standards of three
610 different sizes, from $7.52x10^{-12}$ cm^3 to $2.38x10^{-11}$ cm^3 of ^{84}Kr. For data reduction, only air
611 standards of similar size as the samples were considered. Repeat measurements of the largest air
612 standard size (^{84}Kr of $2.38x10^{-11}$ cm^3) show an even better reproducibility, typically of 2 ‰ for
613 the $^{78}Kr/^{84}Kr$, of 2.5 ‰ for the $^{80}Kr/^{84}Kr$, of 1 ‰ for the $^{82}Kr/^{84}Kr$, of 1.5 ‰ for the $^{83}Kr/^{84}Kr$ and
614 of 1 ‰ for the $^{86}Kr/^{84}Kr$.

615 **Accumulation blank and tests**

616 An important parameter to monitor is the blank of the charcoal trap (see above the total
617 numbers of days the trap remained in static vacuum for each sample). We carried out
618 accumulation blanks consisting in trapping Ar, Kr and Xe from the line in different blank steps,
619 as we did for the crush steps. The accumulated blank represents 3.1 % of the total measured Kr
620 for sample D22B-1, 1.7 % for D22B-2, 1.9 % for D22B-3, 3.7 % for D22A, 2.1 % for DG2017-1
621 and 1.9 % for DG2017-2, with atmospheric isotopic ratios. These blanks represent 3.2 % and 6.7
622 % of the total measured Ar and Xe, respectively, for sample D22B-1, 1.9 % and 3.7 % for D22B-
623 2, 2.1 % and 4.0 % for D22B-3, 3.6 % and 8.0 % for D22A, 3.8 % and 4.8 % for DG2017-1 and
624 1.9 % and 4.0 % for DG2017-2. We corrected the measured argon, krypton and xenon
625 abundances and isotopic ratios for these blanks. This correction is negligible given the blank
626 proportions for each sample.

627 The measured Kr isotopic ratios for the D22 and DG2017 samples are similar, within
628 uncertainties, suggesting that the blank correction is not important for this accumulation

629 procedure, i.e. the quantity of accumulated gas is too large to be affected by the blank. These
630 similar results provide confidence that the procedure is reproducible for precisely measuring
631 small variations in Kr isotopes in such samples in spite of the significant amount of gas
632 processing/distillations.

633 However, the measured krypton and xenon isotopic ratios may be lower limits for the
634 Galápagos and Iceland sources, as for the accumulation protocol we considered crushing steps
635 with $^{20}Ne/^{22}Ne$ lower than the maximum measured value for these sources. The average $^{20}Ne/^{22}Ne$
636 ratios of the accumulated gas for each sample are between 11.99 and 12.41 (Supplementary Table
637 **2**), that is lower than the maximum measured value > 12.8 for these sources. However, as
638 explained in a previous study[8], mixing in a Kr-Ne or Xe-Ne space would be hyperbolic and so
639 crushing steps with lower $^{20}Ne/^{22}Ne$ ratio than the maximum value but higher than 11.75 would
640 still have Kr and Xe isotopic ratios very close to the source value (Extended Data Figure 2).
641 Therefore, we expect the measured krypton and xenon isotopic ratios to be representative of the
642 Galápagos and Iceland sources. As there are no previous krypton isotopic data for high $^{20}Ne/^{22}Ne$
643 ratio for these oceanic islands we cannot correct for this small effect.

644 In addition, we note that the small Kr isotopic differences observed between the four D22
645 and the two DG2017 measurements may be explained either by instrumental variability (as
646 observed with standards) or by small differences in the air-like contaminant (air vs. seawater for
647 instance). More investigation would be needed to determine the cause of these small variations.

648 The neon isotopic ratios fall exactly on the mixing lines previously determined for these
649 samples in other noble gas labs (Supplementary Table 2). This is a further confirmation of the
650 robustness of the measurements by the new 5F5M mass spectrometer. Another important
651 observation is that the measured $^{40}Ar/^{36}Ar$ ratios and the average $^{20}Ne/^{22}Ne$ ratios of the

accumulated gas fall exactly on the mixing hyperbolae previously identified for these samples (Extended Data Figure 5). The $^{129}Xe/^{130}Xe$ and $^{136}Xe/^{130}Xe$ ratios also fall exactly on the trend identified for Iceland[14] (Figure 3), while there is no previously published data for the Galápagos hotspot samples. This is robust evidence that suggests that the accumulation protocol worked very well for these samples and that the measured Kr isotopic ratios are representative of these OIB sources. In Figure 3 panel b, data for upper mantle include MORB from the North Atlantic[8,58–60], Equatorial Atlantic[61] and South West Indian Ridge[33,62], CO_2 well gas[31] and thermal springs from Eifel[32] and Massif Central[63].

However, the Ar abundances and Ar isotopic ratios cannot be taken as representative of the source compositions. As shown in Extended Data Figure 5, the measured $^{40}Ar/^{36}Ar$ ratios with the accumulation protocol are much lower than the highest values determined for these samples. This is due to the principles of the accumulation protocol[8]: mixing in Extended Data Figure 5 is hyperbolic and so accumulating steps with high $^{20}Ne/^{22}Ne$ ratios (>11.75) provides Kr with similar isotopic ratios as the source but Ar with much lower ratios.

We also carried out tests of accumulation with aliquots of air standard. For each of the three tests, three aliquots of $7.52x10^{-12}$ cc of ^{84}Kr were accumulated on the charcoal trap and analyzed as explained above. The measured Kr isotopic ratios for each test, presented in Extended Data Table 5, are similar to measurements of air standard aliquots of $7.52x10^{-12}$ cc and of $2.37x10^{-11}$ cc of ^{84}Kr. The results of these tests argue against mass fractionation induced by the accumulation protocol itself.

Uncertainties on isotopic ratios and discussion of the results

674 The uncertainties on isotopic ratios were calculated by propagation of errors of the
675 measured uncertainty and of the external reproducibility estimated with standards. For each
676 sample, the external reproducibility was estimated by considering a suite of air standards, with
677 similar size as the samples (as explained above), analyzed before and after the sample.
678 The $^{86}Kr/^{84}Kr$ ratios were not corrected for fission production, as it is expected to be
679 negligible. Spontaneous fission of ^{238}U can produce small amounts of ^{83}Kr, ^{84}Kr and ^{86}Kr while
680 spontaneous fission of ^{244}Pu produces ^{86}Kr[64]. The fission yields are 0.95 % and 0.11 % for ^{86}Kr
681 from ^{238}U and ^{244}Pu fissions, respectively[64]. It is important to note that this correction would lower
682 the measured $^{86}Kr/^{84}Kr$ ratio. Therefore, the anomaly observed for ^{86}Kr (Figures 1 and 5) would
683 be even more important with this fissiogenic correction.
684 Another observation that precludes interference on ^{80}Kr from $^{40}Ar_2^+$ is the overall pattern
685 in Figure 1. As the krypton isotopic pattern closely follow that of Phase Q for isotopes of mass
686 78, 80, 82, 83, it is unlikely that any interference with $^{40}Ar_2^+$ on mass 80 occurred. Otherwise, we
687 should observe a noticeable excess for the $^{80}Kr/^{84}Kr$ ratio relative to Phase Q.
688 We also estimated the probabilities that the measured krypton isotopic ratios are identical
689 to air within uncertainties. Considering the six data independently, we calculated the probability
690 that the $^{78}Kr/^{84}Kr$, $^{80}Kr/^{84}Kr$ and $^{82}Kr/^{84}Kr$ ratios are all identical to or higher than air by randomly
691 picking an isotopic ratio based on the measured value and the uncertainty assuming a normal
692 distribution, and comparing it to the atmospheric ratios, also randomly picked according to the
693 normal distribution. We found that the probability that the $^{78}Kr/^{84}Kr$, $^{80}Kr/^{84}Kr$ and $^{82}Kr/^{84}Kr$ ratios
694 are all identical to or higher than air is 0.19% for sample D22B-1, 0% for samples D22B-2,
695 D22B-3 and D22A, 2.19 % for DG2017-1 and 0.38 % for DG2017-2. Similarly, the probabilities
696 that the $^{78}Kr/^{84}Kr$, $^{80}Kr/^{84}Kr$ and $^{82}Kr/^{84}Kr$ ratios are all within uncertainties of air (± 2 sigma) are

0.23% for sample D22B-1, 0.12% for D22B-2, 0% for D22B-3, 0.66% for D22A, 1.5% for DG2017-1 and 0.21% for DG2017-2. The probabilities that all five Kr isotopic ratios are within uncertainties of air (± 2 sigma) are 0.09% for sample D22B-1, 0.002% for D22B-2, 0% for D22B-3, 0.24% for D22A, 0.37% for DG2017-1 and 0.07% for DG2017-2. Therefore, these calculations demonstrate that it is very likely that the measured krypton isotopic compositions are different from air.

Krypton cosmochemistry and compilation of chondrites krypton isotopic data

The krypton isotopic composition of carbonaceous chondrites is a mixture of Phase Q-Kr and Kr from presolar grains such as SiC, which were used to determine the s-process Kr isotopic composition[37,38]. The large variability in δ^{86}Kr of SiC grains are due to the fact that ^{86}Kr is at a branching point on the s-process path and thus, the SiC grain composition is influenced by neutron flux and stellar temperature in individual AGB stars. The Kr isotopic compositions of SiC grains reflect mixtures of the normal "N" component, close to the solar composition, and the "G" component corresponding to s-process Kr and which range in Kr isotopic ratios is predicted by AGB star composition models[38].

We compiled krypton isotopic data from carbonaceous, ordinary and enstatite chondrites (Extended Data Table 3) in order to compare with our new data. We report data only for chondrites of low petrologic types (1 to 3) as they have better preserved their original constituents[65].

We re-determined the Average Carbonaceous Chondrites (AVCC) krypton isotopic composition (Extended Data Table 1 and 3) in order to take into account more data than usually considered and also because it is not always clear in the literature from which data this AVCC

720 composition was calculated. It is often referred for AVCC to the study of Pepin[66] but in this study
721 chondritic krypton is not only calculated with data for carbonaceous chondrites.
722 For the calculation of AVCC, we used data from several studies that have measured the
723 carbonaceous chondrites Murray, Cold Bokkeveld, Orgueil, Lancé and Leoville[67–70]. Some data
724 were not considered because some meteorites were too much affected by krypton from neutron-
725 capture production[71,72].
726 All the data considered were first re-normalized to the atmospheric composition used in
727 this study[73] in case other values were taken. The data for Leoville[69] were corrected considering
728 they were reported to the atmospheric composition of Nier[74] as described in the data table, and
729 not to that of Nief[75] as mentioned in the text.
730 The data for Leoville[69] were corrected for cosmogenic krypton production, for the other
731 carbonaceous meteorites no cosmogenic correction appears necessary[67,68,70]. To correct Leoville
732 data for cosmogenic krypton, we use two methods that give similar results. The first one
733 consisted in using the $^{78}Kr/^{21}Ne$ ratio of the spallation end-member[76] of $7.6x10^{-6}$ and the krypton
734 spallation spectra[77]. The second method consisted in calculating the production ratios of $^{83}Kr/^{21}Ne$
735 for the spallogenic end-member based on determined equations[78] provided that $^{22}Ne/^{21}Ne > 1.08$-
736 1.10[78,79] and combining this production ratio with the krypton spallation spectra[77]. The correction
737 was less than 0.2 % for all isotopic ratios. The data were not corrected for neutron-capture
738 production.
739 The AVCC composition calculated in Extended Data Table **3** represents the weighted
740 mean of the 8 data considered (only 5 data for ^{78}Kr and 6 for ^{80}Kr). The uncertainties reported are
741 the standard error of the mean to take into account the underdispersion/overdispersion of the data.
742 We note that because the Earth accreted substantial amounts of carbonaceous meteorites (~5-15%

743 of bulk Earth mass[5,39]), the average value of the carbonaceous meteorites (AVCC) should be
744 representative of the composition of the carbonaceous meteorites accreted. Consequently, the
745 appropriate parameter for the uncertainty of the average value is the standard error. Our
746 calculated mean value for AVCC composition is consistent with a previous estimation[67].

747 For ordinary chondrites, we selected data from the study of Eugster[80] (Extended Data
748 Table 3), and corrected them for cosmogenic production using their estimated $^{83}Kr/^{21}Ne$[80] and the
749 Kr spallation spectra[77]. We did not report the $^{80}Kr/^{84}Kr$ and $^{82}Kr/^{84}Kr$ ratios as both ratios are
750 clearly affected by neutron-induced production.

751 For enstatite chondrites, we used data from two studies[81,82] and corrected them for
752 cosmogenic production using the Kr spallation spectra[77] and the calculated production ratios $^{83}Kr/$
753 ^{21}Ne for the spallogenic end-member[78]. We only report the $^{83}Kr/^{84}Kr$ and $^{86}Kr/^{84}Kr$ ratios, as the
754 other isotopic ratios show more variability, likely due to imperfect neutron-induced production
755 correction for $^{80}Kr/^{84}Kr$ and $^{82}Kr/^{84}Kr$ ratios and to imperfect cosmogenic correction for the
756 $^{78}Kr/^{84}Kr$ ratio.

757 As for AVCC, the averages for enstatite and ordinary chondrites correspond to the
758 weighted mean and the reduced chi-square of the weighted error.

759

760 **Calculation of the krypton mixing proportions in the OIB sources**

761 To explain the krypton isotopic patterns of the Galápagos and Iceland sources, we
762 considered several mixing combinations (Figure 4). The aim of this approach was to fit the
763 anomalies in $^{78}Kr/^{84}Kr$ and $^{80}Kr/^{84}Kr$, the two ratios most resolvable from the air ratios, to estimate
764 the expected $^{86}Kr/^{84}Kr$ ratio. We used the same methods of linear least square fitting and Monte
765 Carlo for propagation of uncertainties as described for Xe component deconvolution[33].

766 If the composition of Kr in the plume sources is a mixture of AVCC and atmospheric Kr,
767 then 52 ± 8 % of the Kr in the Galápagos plume and 36 ± 8 % of the Kr in the Iceland plume
768 originate from AVCC based on the measured ^{78}Kr-^{80}Kr-^{84}Kr. A solar-AVCC mixture would
769 indicate that at most 10 ± 2 % of the Kr in the Galápagos plume and 16 ± 2 % of the Kr in the
770 Iceland plume would be solar. A phase Q-air mixture would give 100^{0}_{-9} % and 71 ± 17 % of the
771 Kr in the Galápagos and Iceland plumes, respectively, originated from Q.
772 We also tested this approach considering a mixing of AVCC, solar and air krypton to fit
773 the ^{78}Kr/^{84}Kr, ^{80}Kr/^{84}Kr and ^{82}Kr/^{84}Kr ratios. This 3-component mixing gives a similar result for
774 samples D22 as the mixing of AVCC-air krypton, that is 0 % of solar krypton, 48 ± 6 % of
775 AVCC krypton and 52 ± 6 % of air krypton. However, it was not possible to fit well the DG2017
776 sample composition with this three-component mixing given that the measured ^{82}Kr/^{84}Kr ratio for
777 this sample is not as well resolved from air as for samples D22. The fact that this three-
778 component mixing gives the same result than the two-component mixing considering only the
779 ^{78}Kr/^{84}Kr and ^{80}Kr/^{84}Kr ratios for samples D22 suggests that it is a valid approach to only consider
780 these two ratios for the fit and that the solar end-member did not contribute significantly to
781 mantle krypton.
782 The uncertainties on the mixing proportions take into account uncertainties on the
783 measured Kr isotopic ratios for the samples as well as the uncertainties on the AVCC, solar and
784 Phase Q end-members.
785
786
787

Data availability

Geochemical data that support the findings of this study are archived on EarthChem at https://ecl.earthchem.org/view.php?id=2065. Source data are provided with this paper.

Method references

51. Geist, D. *et al.* Submarine Fernandina: Magmatism at the leading edge of the Galapagos hot spot. *Geochemistry, Geophys. Geosystems* **7**, Q12007 (2006).
52. Peterson, M. E. *et al.* Submarine Basaltic Glasses from the Galapagos Archipelago: Determining the Volatile Budget of the Mantle Plume. *J. Petrol.* **58**, 1419–1450 (2017).
53. Graham David, W., Hanan Barry, B., Hémond, C., Blichert-Toft, J. & Albarède, F. Helium isotopic textures in Earth's upper mantle. *Geochemistry, Geophys. Geosystems* **15**, 2048–2074 (2014).
54. Colin, A., Moreira, M., Gautheron, C. & Burnard, P. Constraints on the noble gas composition of the deep mantle by bubble-by-bubble analysis of a volcanic glass sample from Iceland. *Chem. Geol.* **417**, 173–183 (2015).
55. Péron, S., Mukhopadhyay, S. & Huh, M. A new dual stainless steel cryogenic trap for efficient separation of krypton from argon and xenon. *J. Anal. At. Spectrom.* (2020). doi:10.1039/D0JA00052C
56. Lott, D. E. I. I. I. Improvements in noble gas separation methodology: a nude cryogenic trap. *G-cube* **2001GC0002**, (2001).
57. Stanley, R. H. R., Baschek, B., Lott III, D. E. & Jenkins, W. J. A new automated method for measuring noble gases and their isotopic ratios in water samples. *Geochemistry, Geophys. Geosystems* **10**, (2009).
58. Kunz, J., Staudacher, T. & Allègre, C. J. L. B.-K. Plutonium-Fission Xenon Found in Earth's Mantle. *Science* **280**, 877–880 (1998).
59. Moreira, M., Kunz, J. & Allègre, C. J. Rare gas systematics on popping rock : estimates of isotopic and elemental compositions in the upper mantle. *Science* **279**, 1178–1181 (1998).
60. Parai, R. & Mukhopadhyay, S. Heavy noble gas signatures of the North Atlantic Popping Rock 2ΠD43: Implications for mantle noble gas heterogeneity. *Geochim. Cosmochim. Acta* **294**, 89–105 (2021).
61. Tucker, J. M., Mukhopadhyay, S. & Schilling, J.-G. The heavy noble gas composition of the depleted {MORB} mantle ({DMM}) and its implications for the preservation of heterogeneities in the mantle. *Earth Planet. Sci. Lett.* **355--356**, 244–254 (2012).
62. Parai, R., Mukhopadhyay, S. & Standish, J. J. Heterogeneous upper mantle Ne, Ar and Xe isotopic compositions and a possible Dupal noble gas signature recorded in basalts from the Southwest Indian Ridge. *Earth Planet. Sci. Lett.* **359–360**, 227–239 (2012).
63. Moreira, M., Rouchon, V., Muller, E. & Noirez, S. The xenon isotopic signature of the mantle beneath Massif Central. *Geochemical Perspect. Lett.* **6**, 28–32 (2018).
64. Ozima, M. & Podosek, F. A. *Noble Gas Geochemistry*. (Cambridge University Press, 2002).

65. Huss, G. R. & Lewis, R. S. Presolar diamond, SiC, and graphite in primitive chondrites: abundances as a function of meteorite class and petrologic type. *Geochim. Cosmochim. Acta* **59**, 115–160 (1995).
66. Pepin, R. O. On Noble Gas Processing in the Solar Accretion Disk. *Space Sci. Rev.* **106**, 211–230 (2003).
67. Eugster, O., Eberhardt, P. & Geiss, J. Krypton and xenon isotopic composition in three carbonaceous chondrites. *Earth Planet. Sci. Lett.* **3**, 249–257 (1967).
68. Marti, K. Isotopic composition of trapped krypton and xenon in chondrites. *Earth Planet. Sci. Lett.* **3**, 243–248 (1967).
69. Manuel, O. K., Wright, R. J., Miller, D. K. & Kuroda, P. K. Heavy noble gases in Leoville: The case for mass fractionated xenon in carbonaceous chondrites. *J. Geophys. Res.* **75**, 5693–5701 (1970).
70. Krummenacher, D., Merrihue, C. M., Pepin, R. O. & Reynolds, J. H. Meteoritic krypton and barium versus the general isotopic anomalies in meteoritic xenon. *Geochim. Cosmochim. Acta* **26**, 231–249 (1962).
71. Manuel, O. K., Wright, R. J., Miller, D. K. & Kuroda, P. K. Isotopic compositions of rare gases in the carbonacaous chondrites Mokoia and Allende. *Geochim. Cosmochim. Acta* **36**, 961–983 (1972).
72. Matsuda, J.-I., Lewis, R. S., Takahashi, H. & Anders, E. Isotopic anomalies of noble gases in meteorites and their origins---VII. C3V carbonaceous chondrites. *Geochim. Cosmochim. Acta* **44**, 1861–1874 (1980).
73. Basford, J. R., Dragon, J. C., Pepin, R. O., Coscio Jr., M. R. & Murthy, V. R. Krypton and xenon in lunar fines. in *Lunar and Planetary Science Conference Proceedings* **4**, 1915–1955 (1973).
74. Nier, A. O. A redetermination of the relative abundances of the isotopes of neon, krypton, rubidium, xenon and mercury. *Phys. Rev.* **79**, 450–454 (1950).
75. Nief, G. (as reported un isotopic abundance ratios given for reference samples stocked by the National Bureau of Standards). *NBS Tech. Note 51* edited by F. Mohler (1960).
76. Eugster, O., Eberhardt, P. & Geiss, J. The isotopic composition of krypton in unequilibrated and gas rich chondrites. *Earth Planet. Sci. Lett.* **2**, 385–393 (1967).
77. Marti, K., Eberhardt, P. & Geiss, J. Spallation, Fission, and Neutron Capture Anomalies in Meteoritic Krypton and Xenon. *Zeitschrift für Naturforsch. A* **21**, 398–426 (1966).
78. Eugster, O. Cosmic-ray production rates for 3He, 21Ne, 38Ar, 83Kr, and 126Xe in chondrites based on 81Kr-Kr exposure ages. *Geochim. Cosmochim. Acta* **52**, 1649–1662 (1988).
79. Wieler, R. Cosmic-Ray-Produced Noble Gases in meteorites. *Rev. Mineral. Geochemistry* **47**, 125–170 (2002).
80. Eugster, O., Eberhardt, P. & Geiss, J. Isotopic analyses of krypton and xenon in fourteen stone meteorites. *J. Geophys. Res.* **74**, 3874–3896 (1969).
81. Nakashima, D. & Nakamura, T. Trapped noble gas components and exposure history of the enstatite chondrite ALH84206. *Geochem. J.* **40**, 543–555 (2006).
82. Okazaki, R., Takaoka, N., Nagao, K. & Nakamura, T. Noble gases in enstatite chondrites released by stepped crushing and heating. *Meteorit. Planet. Sci.* **45**, 339–360 (2010).
83. Heber, V. S. *et al.* Isotopic fractionation of solar wind: evidence from fast and slow solar wind collected by the Genesis Mission. *Astrophys. J.* **759**, 121–133 (2012).

84. Pepin, R. O., Schlutter, D. J., Becker, R. H. & Reisenfeld, D. B. Helium, neon, and argon composition of the solar wind as recorded in gold and other Genesis collector materials. *Geochim. Cosmochim. Acta* **89**, 62–80 (2012).

Acknowledgements

The authors thank Michael Huh for assistance in the lab as well as Magdalena Huyskens, Sarah Stewart and Simon J. Lock for helpful discussions and comments on the manuscript. Helium isotope analyses in the OSU noble gas lab were supported by NSF 1763255. Collection of the Fernandina samples and WHOI participation was supported by NSF Ocean Sciences.

Author contributions

S.P. and S.M. designed the study. S.P. made the noble gas (Ne, Ar, Kr, Xe) analyses, interpreted the data and wrote the manuscript with feedback from S.M. M.D.K. and D.W.G. provided the samples, discussed results and contributed to final manuscript preparation. D.W.G. made the He and CO_2 analyses of sample DG2017.

Competing interests

The authors declare no competing interests.

Correspondence and requests for materials should be addressed to S.P.

Extended Data Table 1: Krypton isotopic compositions of samples AHA-NEMO2-D22A and AHA-NEMO2-D22B (hereafter D22A and D22B, Fernandina, Galápagos, respectively) and DG2017 (Midfell, Iceland). The weighted averages of the four Galápagos and the two Iceland measurements are reported. Compositions of Air[73], Average Carbonaceous Chondrites (AVCC), Phase Q[25] and Solar Wind[24] are indicated as comparison. ^{84}Kr is reported as the total amount measured in cm^{3}STP and not divided by the sample mass. Sample D22B-1 was 4.04599g, D22B-2 4.09500 g, D22B-3 3.0052 g, D22A 4.1554 g, DG2017-1 4.5371 g and DG2017-2 4.7092g. Refer to text and Extended Data Table 3 for the calculation of the AVCC end-member. Uncertainties are 1□.

Sample	^{84}Kr ($\times 10^{-11}$ cm^{3}STP)	^{78}Kr/^{84}Kr	^{80}Kr/^{84}Kr	^{82}Kr/^{84}Kr	^{83}Kr/^{84}Kr	^{86}Kr/^{84}Kr
D22B-1	1.61	0.00602	0.03941	0.2021	0.2016	0.3053
+/-	0.02	0.00003	0.00017	0.0005	0.0004	0.0006
D22B-2	3.10	0.00603	0.03941	0.2015	0.2017	0.3065
+/-	0.05	0.00003	0.00020	0.0004	0.0004	0.0004
D22B-3	2.30	0.00601	0.03894	0.2006	0.2006	0.3070
+/-	0.04	0.00004	0.00017	0.0005	0.0003	0.0007
D22A	1.22	0.00604	0.03956	0.2023	0.2015	0.3053
+/-	0.04	0.00005	0.00019	0.0006	0.0004	0.0007
D22 (average)		**0.00603**	**0.03932**	**0.2016**	**0.2012**	**0.3061**
+/-		**0.00002**	**0.00009**	**0.0002**	**0.0002**	**0.0003**
DG2017-1	2.19	0.00605	0.03949	0.2024	0.2016	0.3059
+/-	0.04	0.00003	0.00012	0.0003	0.0003	0.0004
DG2017-2	2.42	0.00601	0.03947	0.2019	0.2013	0.3056
+/-	0.08	0.00004	0.00021	0.0006	0.0004	0.0007
DG2017 (average)		**0.00604**	**0.03948**	**0.2023**	**0.2015**	**0.3058**
+/-		**0.00002**	**0.00011**	**0.0002**	**0.0003**	**0.0004**
Air		0.00609	0.03960	0.2022	0.2014	0.3052
AVCC		0.00595	0.03928	0.2008	0.2007	0.3092
+/-		0.00002	0.00006	0.0003	0.0002	0.0002
Phase Q		0.00603	0.03937	0.2018	0.2018	0.3095
+/-		0.00003	0.00007	0.0002	0.0002	0.0005
Solar Wind		0.00642	0.04120	0.2054	0.2034	0.3012
+/-		0.00005	0.00020	0.0002	0.0002	0.0004

Extended Data Table 2: Xenon abundances and isotopic ratios measured with the accumulation protocol for the Galápagos (AHA-NEMO2-D22A and AHA-NEMO2-D22B) and Iceland (DG2017) samples. Uncertainties are 1σ.

Sample	^{130}Xe x10^{-13} cm^3STP	$^{124}Xe/^{130}Xe$	$^{126}Xe/^{130}Xe$	$^{128}Xe/^{130}Xe$	$^{129}Xe/^{130}Xe$	$^{131}Xe/^{130}Xe$	$^{132}Xe/^{130}Xe$	$^{134}Xe/^{130}Xe$	$^{136}Xe/^{130}Xe$
D22B-1	1.57	0.0236	0.0215	0.4723	6.66	5.23	6.65	2.59	2.23
+/-	0.04	0.0006	0.0006	0.0033	0.03	0.02	0.03	0.01	0.01
D22B-2	3.05	0.0231	0.0212	0.4768	6.61	5.23	6.63	2.59	2.21
+/-	0.07	0.0006	0.0005	0.0030	0.03	0.04	0.04	0.03	0.01
D22B-3	1.97	0.0234	0.0223	0.4740	6.63	5.23	6.65	2.60	2.23
+/-	0.04	0.0007	0.0007	0.0035	0.03	0.02	0.03	0.01	0.01
D22A	1.13	0.0227	0.0218	0.4695	6.70	5.20	6.63	2.61	2.22
+/-	0.06	0.0007	0.0006	0.0034	0.05	0.04	0.04	0.02	0.02
D22 (average)		**0.0232**	**0.0216**	**0.4734**	**6.64**	**5.22**	**6.64**	**2.60**	**2.22**
+/-		**0.0003**	**0.0003**	**0.0016**	**0.02**	**0.01**	**0.02**	**0.01**	**0.01**
DG2017-1	2.37	0.0236	0.0223	0.4715	6.74	5.23	6.64	2.62	2.25
+/-	0.04	0.0004	0.0005	0.0024	0.04	0.03	0.03	0.02	0.01
DG2017-2	2.31	0.0241	0.0224	0.4754	6.79	5.22	6.66	2.62	2.26
+/-	0.07	0.0008	0.0008	0.0036	0.03	0.03	0.03	0.01	0.01
DG2017 (average)		**0.0237**	**0.0223**	**0.4727**	**6.78**	**5.22**	**6.65**	**2.62**	**2.25**
+/-		**0.0004**	**0.0004**	**0.0020**	**0.03**	**0.02**	**0.02**	**0.01**	**0.01**
Air		0.0234	0.0218	0.4710	6.50	5.21	6.61	2.56	2.18

Extended Data Table 3: Compilation of carbonaceous, ordinary and enstatite chondrites krypton isotopic data[67–70,80–82]. Data are normalized to the atmospheric composition used in this study[73]. The Leoville data[69], ordinary[80] and enstatite chondrites[81,82] data were corrected for cosmogenic component (refer to the Method section for details).

Meteorites	Class	$^{78}Kr/^{84}Kr$	σ	$^{80}Kr/^{84}Kr$	σ	$^{82}Kr/^{84}Kr$	σ	$^{83}Kr/^{84}Kr$	σ	$^{86}Kr/^{84}Kr$	σ
Carbonaceous chondrites (CC)											
Murray[68]	CM2	0.00594	0.00009	0.03938	0.00053	0.2006	0.0020	0.2009	0.0018	0.3093	0.0019
Murray[70]	CM2					0.1988	0.0016	0.1994	0.0014	0.3068	0.0024
Cold Bokkeveld[67]	CM2	0.00597	0.00004	0.03915	0.00030	0.2013	0.0008	0.2014	0.0009	0.3092	0.0008
Orgeuil[70]	CI1					0.1998	0.0012	0.2001	0.0012	0.3091	0.0015
Orgeuil[67]	CI1	0.00588	0.00008	0.03922	0.00042	0.2011	0.0016	0.2011	0.0016	0.3090	0.0015
Lance[68]	CO3.5	0.00591	0.00011	0.03948	0.00059	0.2006	0.0026	0.2013	0.0024	0.3093	0.0029
Lance[67]	CO3.5	0.00600	0.00008	0.03958	0.00046	0.2017	0.0015	0.2013	0.0014	0.3099	0.0012
Leoville[69]	CV3			0.03824	0.00030	0.2009	0.0012	0.2005	0.0010	0.3090	0.0010
AVCC		**0.00595**	**0.00002**	**0.03928**	**0.00006**	**0.2008**	**0.0003**	**0.2007**	**0.0002**	**0.3092**	**0.0002**
Ordinary chondrites (OC)											
Dimmitt[80]	H3.7	0.00583	0.00023					0.2019	0.0040	0.3089	0.0038
Mezö Madaras[80]	L3.5	0.00591	0.00017					0.2014	0.0027	0.3112	0.0029
Parnallee[80]	LL3	0.00595	0.00010					0.2021	0.0016	0.3104	0.0029
Tieschitz 1[80]	H3.6	0.00599	0.00017					0.2012	0.0036	0.3105	0.0029
Tieschitz 4[80]	H3.6	0.00605	0.00006					0.2013	0.0013	0.3088	0.0014
Average OC		**0.00601**	**0.00003**					**0.2016**	**0.0002**	**0.3097**	**0.0005**
Enstatite chondrites (EC)											
ALH84206[81]	EH3							0.2020	0.0010	0.3070	0.0010
ALH 77295[82]	EH3							0.2026	0.0004	0.3124	0.0005
Sahara 97096[82]	EH3							0.2020	0.0005	0.3102	0.0006
Y-691[82]	EH3							0.2034	0.0004	0.3142	0.0004
Y-792959[82]	EH3							0.2014	0.0004	0.3113	0.0005
Y-793161[82]	EH3							0.2017	0.0004	0.3094	0.0006
Average EC								**0.2022**	**0.0003**	**0.3118**	**0.0008**

Extended Data Table 4: Argon abundances and isotopic ratios measured with the accumulation protocol for the Galápagos (AHA-NEMO2-D22A and AHA-NEMO2-D22B) and Iceland (DG2017) samples. As mentioned in the text, the values for argon cannot be used as representative of the source compositions. Uncertainties are 1□.

Sample	^{36}Ar x10^{-10} cm^{3}STP	σ	^{38}Ar/^{36}Ar	σ	^{40}Ar/^{36}Ar	σ
AHA-NEMO2-D22B-1	5.75	0.10	0.1879	0.0003	1902.6	1.0
AHA-NEMO2-D22B-2	9.73	0.20	0.1885	0.0003	1464.2	1.0
AHA-NEMO2-D22B-3	8.26	0.02	0.1884	0.0003	1347.2	1.0
AHA-NEMO2-D22A	4.25	0.03	0.1879	0.0003	2195.4	1.0
DG2017-1	5.01	0.02	0.1880	0.0004	3025.2	1.0
DG2017-2	7.95	0.05	0.1889	0.0002	3228.8	1.0
Air			0.1880		295.5	

Extended data Table 5: Results of the accumulation tests with air standard aliquots of 7.52x10^{-12} cc of ^{84}Kr. Each test consists of the accumulation of three air standard aliquots of 7.52x10^{-12} cc of ^{84}Kr. The test results are compared with measurements of air aliquots of 7.52x10^{-12} cc (average of n = 16 analyses) and of 2.37x10^{-11} cc (average of n = 5 analyses) of ^{84}Kr. The measured Kr isotopic ratios from the accumulation tests are similar to the ones for air standard aliquots of 7.52x10^{-12} cc and of 2.37x10^{-11} cc of ^{84}Kr.

	^{78}Kr/^{84}Kr	s	^{80}Kr/^{84}Kr	s	^{82}Kr/^{84}Kr	s	^{83}Kr/^{84}Kr	s	^{86}Kr/^{84}Kr	s
Test 1	0.00606	0.00003	0.04010	0.00007	0.2030	0.0002	0.2020	0.0002	0.2900	0.0003
Test 2	0.00611	0.00003	0.04006	0.00007	0.2034	0.0002	0.2021	0.0002	0.2907	0.0002
Test 3	0.00607	0.00003	0.04004	0.00008	0.2033	0.0002	0.2022	0.0002	0.2903	0.0002
Average	0.00608	0.00003	0.04007	0.00003	0.2032	0.0002	0.2021	0.0001	0.2903	0.0004
Average 7.52x10^{-12} cc of ^{84}Kr (n = 16)	0.00609	0.00003	0.04021	0.00010	0.2036	0.0004	0.2022	0.0003	0.2902	0.0003
Measurements of air standard of 2.37x10^{-11} cc of ^{84}Kr										
STD 1	0.00611	0.00002	0.04023	0.00009	0.2033	0.0002	0.2025	0.0002	0.2903	0.0002
STD 2	0.00608	0.00002	0.04034	0.00006	0.2037	0.0002	0.2024	0.0002	0.2903	0.0002
STD 3	0.00612	0.00003	0.04034	0.00006	0.2036	0.0003	0.2023	0.0003	0.2901	0.0002
STD 4	0.00606	0.00002	0.04011	0.00007	0.2031	0.0002	0.2023	0.0002	0.2902	0.0002
STD 5	0.00611	0.00003	0.04019	0.00008	0.2030	0.0002	0.2024	0.0002	0.2905	0.0003
Average (n = 5)	0.00610	0.00003	0.04024	0.00010	0.2033	0.0003	0.2024	0.0001	0.2903	0.0001

Extended Data Figure 1: Krypton isotopic patterns for each analysis. Isotopic ratios are in delta notation □^{i}Kr = ((^{i}Kr/^{84}Kr)$_{sample}$ / (^{i}Kr/^{84}Kr)$_{air}$ -1) x 10^3. a) Sample D22B-1, b) sample D22B-2, c) sample D22B-3, d) sample D22A, e) samples DG2017-1 and DG2017-2. Patterns of Solar Wind[24], Average Carbonaceous Chondrites (AVCC) and Phase Q[25] are shown for reference.

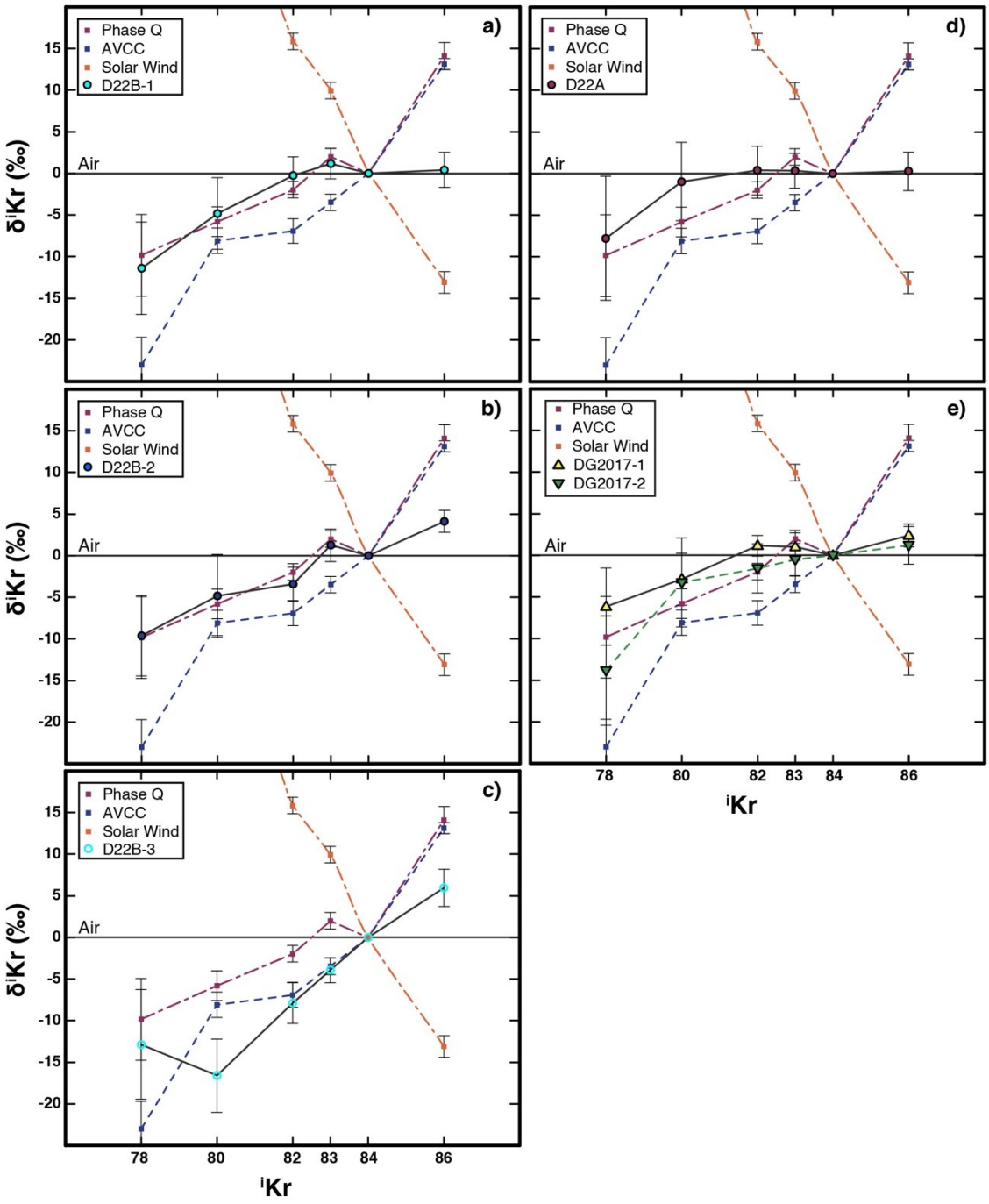
a)
Phase Q
AVCC
Solar Wind
D22B-1
Air
b)
Phase Q
AVCC
Solar Wind
D22B-2
Air
c)
Phase Q
AVCC
Solar Wind
D22B-3
Air
d)
Phase Q
AVCC
Solar Wind
D22A
Air
e)
Phase Q
AVCC
Solar Wind
DG2017-1
DG2017-2
Air
δ^iKr (‰)
15
10
5
0
-5
-10
-15
-20
78
80
82
83
84
86
^iKr

Extended Data Figure 2: Krypton-neon isotope plot. The krypton isotopic compositions of the Galápagos and Iceland mantle sources are not precisely known, our data represent lower limit as explained in the Method. As such, a range is indicated for the deep mantle spanning the Phase Q and AVCC Kr isotopic compositions. The mixing hyperbolae show that accumulating crushing steps with $^{20}Ne/^{22}Ne$ ratios >11.75 allow to obtain Kr isotopic ratios close to the mantle source ratios.

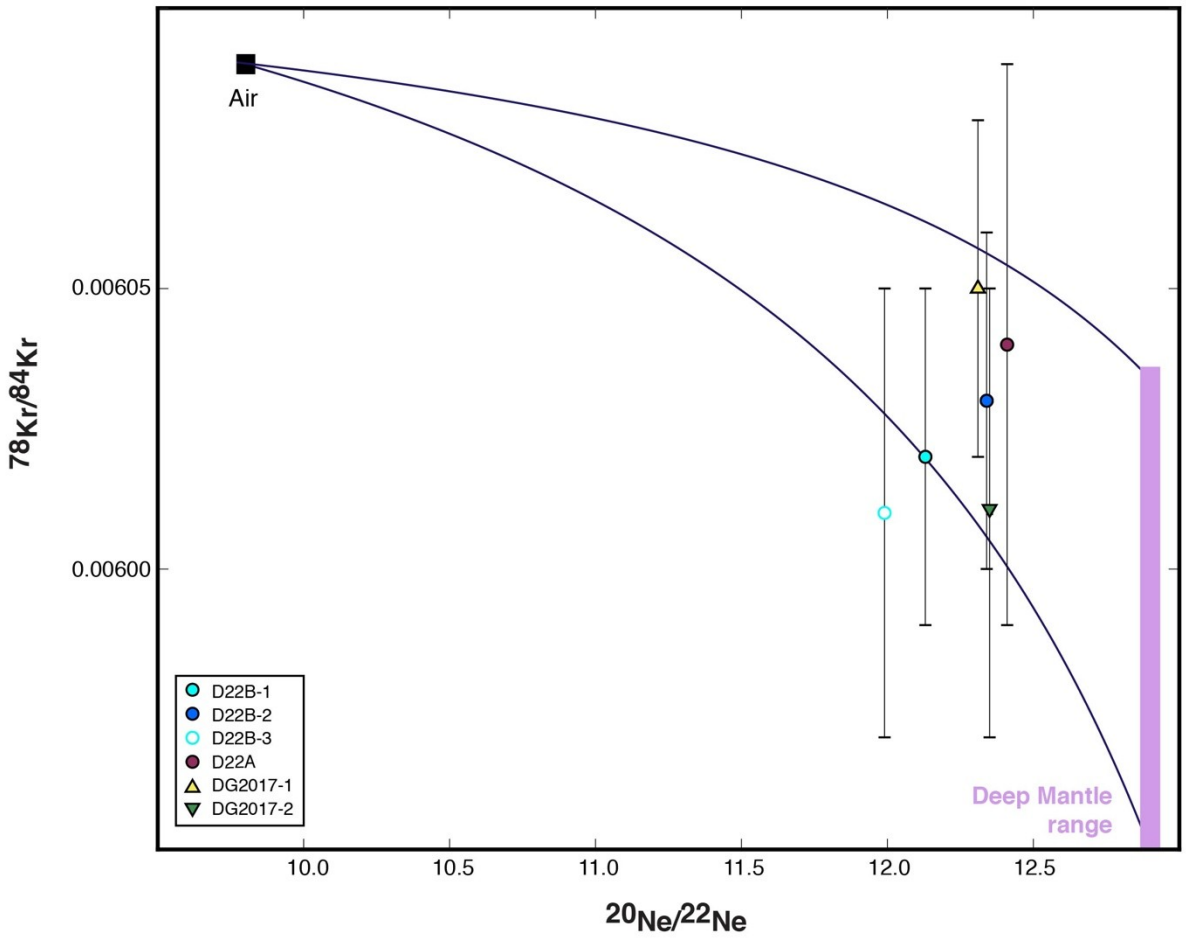

Extended Data Figure 3: Estimation of the probability of the observed deficit in ^{86}Kr for the D22 (Galápagos) and DG2017 (Iceland) samples. The black rectangle represents the probability (0.01 %) that both measured $^{86}Kr/^{84}Kr$ ratios for the Galápagos and Iceland plume sources are higher than the predicted values (Figure 5). The white rectangle represents the probability that both measured ratios are lower than the predicted values, the blue rectangle that the measured ratio for the Galápagos source is lower than the predicted value with the measured ratio for Iceland being higher than the predicted value, and the green rectangle that the measured ratio for the Iceland source is lower than the predicted value with the measured ratio for Galápagos being higher than the predicted value. There is a 99.9 % probability that the Earth's deep mantle has a deficit in ^{86}Kr relative to AVCC.

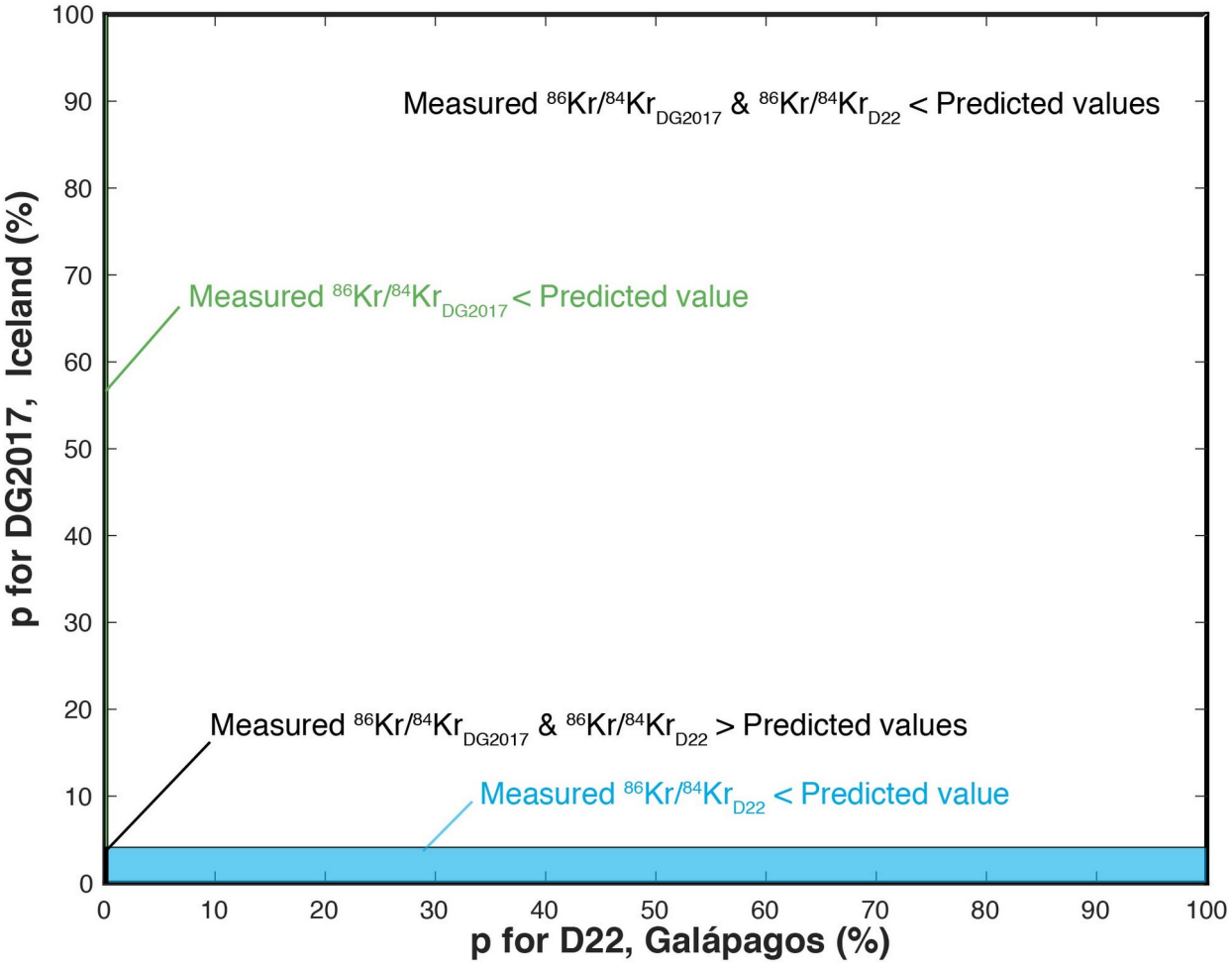

Extended Data Figure 4: Reproducibility of the air standard for krypton isotopic ratios. a) $^{78}Kr/^{84}Kr$, b) $^{80}Kr/^{84}Kr$, c) $^{82}Kr/^{84}Kr$, d) $^{83}Kr/^{84}Kr$ and e) $^{86}Kr/^{84}Kr$. This set of standards was measured over 13 days and include three sizes of air standard, ranging from $7.52x10^{-12}$ cc to $2.37x10^{-11}$ cc of ^{84}Kr. For the samples, only one size of the air standard was used (^{84}Kr of $2.37x10^{-11}$ cc), measurements of this air standard size show an even better reproducibility (typically of 2 ‰ for the $^{78}Kr/^{84}Kr$, of 2.5 ‰ for the $^{80}Kr/^{84}Kr$, of 1 ‰ for the $^{82}Kr/^{84}Kr$, of 1.5 ‰ for the $^{83}Kr/^{84}Kr$ and of 1 ‰ for the $^{86}Kr/^{84}Kr$).

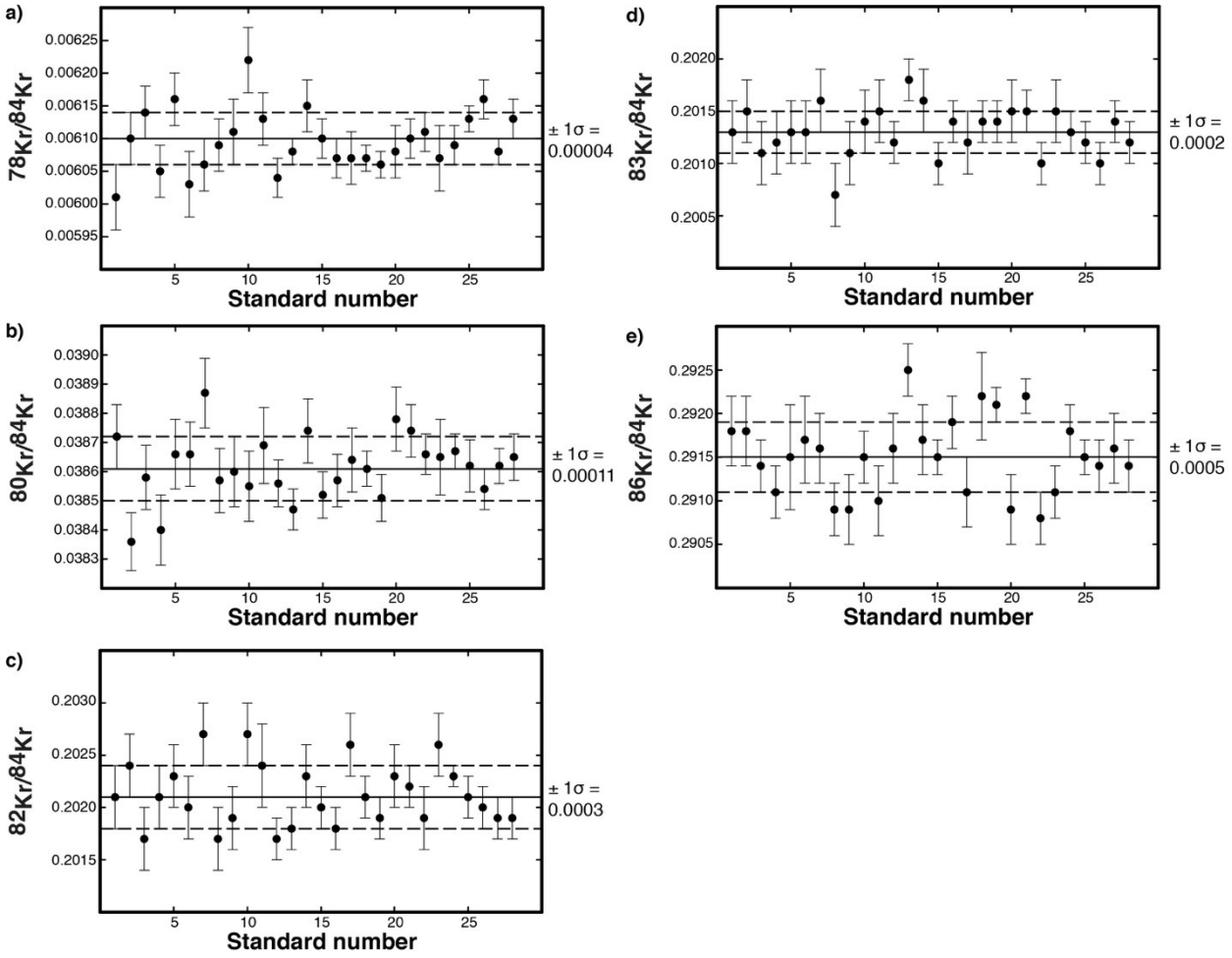

Extended Data Figure 5: Three neon isotope plot for the step-crushing analyses and argon-neon isotope plot for the accumulated gas. a) Neon isotopic ratios for sample D22B-1, D22B-2, D22B-3 and D22A (Galápagos), compared with literature data[11], b) neon isotopic ratios for DG2017-1 and DG2017-2 (Iceland), compared with literature data[14,15,54]. Supplementary Table 2 indicates for which step heavy noble gases were accumulated. Neon-B[4], Sun[83], Solar Wind[84]. c) $^{40}Ar/^{36}Ar$ vs $^{20}Ne/^{22}Ne$ for samples D22B-1, D22B-2, D22B-3 and D22A (Galápagos), in comparison with literature data[11], d) $^{40}Ar/^{36}Ar$ vs $^{20}Ne/^{22}Ne$ for DG2017-1 and DG2017-2 (Iceland) compared with literature data[14,15,54]. The $^{20}Ne/^{22}Ne$ ratios for samples D22B-1, D22B-2, D22B-3, D22A, DG2017-1 and DG2017-2 are the average ratios of the accumulated steps, refer to Supplementary Table 2. The measured $^{40}Ar/^{36}Ar$ ratios as well as the average $^{20}Ne/^{22}Ne$ ratios are consistent with previous measurements for these same samples.